

Water Resources Research



RESEARCH ARTICLE

10.1029/2022WR033453

Cycles-L: A Coupled, 3-D, Land Surface, Hydrologic, and Agroecosystem Landscape Model

Yuning Shi¹ , Felipe Montes¹ , and Armen R. Kemanian¹ 

¹Department of Plant Science, The Pennsylvania State University, University Park, PA, USA

Key Points:

- Cycles-L is a coupled agroecosystem hydrologic modeling system that couples an agroecosystem model with a 3-D land surface hydrologic model
- Cycles-L simulated well stream discharge, grain crops yield, and nitrogen exports in the stream at a 730-ha agricultural experimental watershed
- Cycles-L can simulate landscape level processes affected by climate, topography, soil heterogeneity, and management practices

Correspondence to:

A. R. Kemanian,
kxa15@psu.edu

Citation:

Shi, Y., Montes, F., & Kemanian, A. R. (2023). Cycles-L: A coupled, 3-D, land surface, hydrologic, and agroecosystem landscape model. *Water Resources Research*, 59, e2022WR033453. <https://doi.org/10.1029/2022WR033453>

Received 12 AUG 2022

Accepted 28 JUL 2023

Corrected 6 MAY 2024

This article was corrected on 6 MAY 2024. See the end of the full text for details.

Author Contributions:

Conceptualization: Yuning Shi, Armen R. Kemanian

Data curation: Felipe Montes

Formal analysis: Yuning Shi, Armen R. Kemanian

Funding acquisition: Armen R. Kemanian

Investigation: Yuning Shi, Armen R. Kemanian

Methodology: Yuning Shi, Armen R. Kemanian

Project Administration: Armen R. Kemanian

© 2023. The Authors.

This is an open access article under the terms of the [Creative Commons Attribution-NonCommercial-NoDerivs License](https://creativecommons.org/licenses/by/4.0/), which permits use and distribution in any medium, provided the original work is properly cited, the use is non-commercial and no modifications or adaptations are made.

Abstract Managing landscapes to increase agricultural productivity and environmental stewardship can be informed by spatially-distributed models that operate at spatial and temporal scales that are intervention-relevant. This paper presents Cycles-L, a landscape-scale agroecosystem and hydrologic modeling system, using as a test case a watershed in Pennsylvania. Cycles-L emerges from melding the landscape and hydrology structure of Flux-PIHM, a 3-D land surface hydrologic model, with the agroecosystem processes in the Cycles model. Consequently, Cycles-L can simulate processes affected by topography, soil heterogeneity, and management practices, owing to its physically-based hydrology that can simulate horizontal and vertical transport of solutes with water. The model was tested at a 730-ha experimental watershed within the Mahantango Creek watershed. Cycles-L simulated well stream water and mineral nitrogen discharge (Nash-Sutcliffe coefficient 0.55 and 0.60, respectively) and grain yield (root mean square error 1.2 Mg ha⁻¹). Cycles-L outputs are as good or better than those obtained with the uncoupled Flux-PIHM (water discharge) and Cycles (grain yield) models. Modeled spatial patterns of nitrogen fluxes like denitrification illustrate the combined control of crop management and topography. For example, denitrification is almost twice as high when simulated with Cycles-L than when simulated with Cycles 1-D. Due to its spatial and temporal resolution, Cycles-L fills a gap in the availability of models that operate at a scale relevant to evaluate interventions in the landscape. Cycles-L can become a central component in tools for climate change scenario analysis, precision agriculture, precision conservation, and artificial intelligence-based decision support systems.

1. Introduction

Managing landscapes to increase agricultural productivity and environmental stewardship requires both understanding and representing landscape attributes with ever increasing fidelity. Specifically, the ability to represent the spatial variability and temporal dynamics of water and nutrient flows in such landscapes through spatially-distributed models can help designing cost-effective interventions in the realms of precision agriculture, precision conservation, or watershed management (Beaujouan et al., 2001; Booker et al., 2014; Stöckle et al., 2014). Two features are critical for these models to be applicable in a context of ever more available data. First, they must integrate the wealth of real-time data incoming from in situ sensors, proximal sensing from unmanned vehicles, remote sensing from satellites, and constantly refined land data (e.g., the Soil Survey Geographic Database or SSURGO and the National Land Cover Database or NLCD) and meteorological data such as the Global Land Data Assimilation System (GLDAS; Rodell et al., 2004) and Europe's World Climate Research Program Coordinated Regional Downscaling Experiment (EURO-CORDEX; Jacob et al., 2014). Second, these models must operate at a scale of relevance to represent interventions and with minimal supervision, so that they do not become “mathematical marionettes” (Kirchner, 2006). There are to our knowledge only partial efforts at integrating models and data in this manner; the most advanced models in hydrology include Flux-PIHM (Shi et al., 2013) and ParFlow (Kuffour et al., 2020). This paper presents the model Cycles-L, where L stands for landscape. Cycles-L integrates Flux-PIHM (Shi et al., 2013), a 3-D land surface and hydrologic model, and the Cycles agroecosystem model (Kemanian et al., 2022).

One-dimensional cropping system models are established tools for planning and decision making in agricultural systems with low spatial variability and high quality input data (e.g., Boote et al., 2010; Stöckle & Kemanian, 2020; Zhai et al., 2020). The application of these 1-D models in precision agriculture falls short of their potential (Stafford, 2000). Among other limitations listed by Zhai et al. (2020), this is due to the contrived representation of spatially varying static and dynamic properties. Although these models are often used in a gridded manner in an attempt to represent spatial heterogeneity (e.g., Basso et al., 2007; Batchelor et al., 2002; Saarikko, 2000), their 1-D nature and absence of lateral water and nutrient transport between grids significantly

Resources: Felipe Montes
Software: Yuning Shi, Armen R. Kemanian
Supervision: Armen R. Kemanian
Validation: Yuning Shi, Armen R. Kemanian
Visualization: Yuning Shi
Writing – original draft: Yuning Shi, Felipe Montes
Writing – review & editing: Yuning Shi, Felipe Montes, Armen R. Kemanian

restricts their capacity to depict nonlinearities in water and nutrient availability caused by topography and soil heterogeneity. For example, Shi et al. (2018) compared a spatially-distributed hydrologic and biogeochemistry model that incorporated both lateral water and nutrient transport with a model solely considering lateral water transport but without lateral nutrient transport. They found that the simulation of lateral nutrient transport is critical to accurately capture the spatial distribution of aboveground and soil carbon within a first-order watershed.

Efforts have been made to develop models that represent spatial and temporal variability in a semi-distributed fashion, both in non-agricultural (Tague & Band, 2004) and agricultural landscapes, without resorting to computationally costly numerical solutions of water flow in landscapes. For example, the Soil Water Assessment Tool (SWAT; Arnold et al., 1998) and the Agricultural Policy EXtender (APEX; Gassman et al., 2010) partition the model domain into subareas known as Hydrological Response Units (HRUs), based on terrain or soil attributes. Within HRUs, processes are simulated using the core of the 1-D EPIC model (J. R. Williams, 1990). In the SWAT model, HRUs do not interact; instead, the water, nutrient, and sediment runoff contributions of an HRU to the corresponding watershed outlet are represented through HRU-specific delivery ratios. However, sediment generation and delivery, for example, are not uniformly scaled to the HRU area, which causes output variations solely dependent on the HRU delineation scheme (E. Chen & Mackay, 2004). In the APEX model, the HRUs (or subareas) are hydrologically connected, but the landscape segmentation methodology is ad hoc (Kemanian et al., 2009), calibration requirements are substantial (X. Wang et al., 2011), and the calibration parameters are not necessarily robust (Francesconi et al., 2014; Van Liew et al., 2017).

These challenges are not unique to these modeling systems but are easily overlooked and difficult to grasp without extensive training, as alluded to by Confalonieri et al. (2016). Furthermore, models that aggregate large spatial scales can represent some processes very well (Arnold et al., 1998; Koch et al., 2016), but struggle to capture highly non-linear processes controlled by heterogeneity in topography, soil, and landcover within subareas. Both Stöckle and Kemanian (2020) and Tenreiro et al. (2020) concluded that the representation of landscape processes that affect surface inflow and subsurface lateral flows of water and other constituents is one of the most promising areas for improving current cropping system models. Although efforts in this direction have been underway for decades (e.g., Beaujouan et al., 2001), the usage of spatially-distributed models remains limited. Therefore, a robust, scale-independent formulation of routing is desirable to reduce uncertainty and reliance on local calibration.

Advancements in computational power and modeling techniques have paved the way to the development of coupled agroecosystem hydrologic models. The Precision Agricultural-Landscape Modeling System (PALMS; Molling et al., 2005) combines an enhanced 2-D diffusive wave runoff model with a 1-D biophysical model based on the Integrated BIOSphere Simulator (IBIS; Foley et al., 1996; Kucharik et al., 2000). PALMS has been used to simulate crop and erosion processes (e.g., Bonilla et al., 2007, 2008; Molling et al., 2005), and connected to other crop models (e.g., PALMScot; Booker et al., 2014; Booker et al., 2015). However, while PALMS grids are hydrologically connected at the surface, the distribution of subsurface water is empiric and subsurface lateral flow is not explicitly simulated.

To improve groundwater processes, Kim et al. (2008) integrated the semi-distributed SWAT model with the fully-distributed groundwater model MODFLOW by exchanging SWAT HRUs with MODFLOW grid cells. The SWAT-MODFLOW model was also coupled with the RT3D groundwater solute reactive transport model (Wei et al., 2019). Ward et al. (2018) introduced CropSyst-Microbasin (CS-MB), a spatially-distributed and 3-D hydrologic cropping system model, which added the subsurface lateral flow of the Soil Moisture Routing model to CropSyst. The model was tested in a 10.9-ha watershed growing rainfed wheat in the Inland Pacific Northwest, USA, showing promising potential to simulate field-scale spatial variability of water distribution and grain yield. However, the kinematic assumption used by this model, where the hydraulic gradient for subsurface water flow follows the land slope rather than the water table slope, limits its applicability on gentle slopes (Wigmosta & Lettenmaier, 1999).

Beyond assessing crop production, comprehensive models are needed to track dynamic processes that reshape the landscape such as soil erosion and deposition (Pineux et al., 2017), changes in soil organic carbon stocks (Baker et al., 2007), and the provision of ecosystem services influenced by landscape diversity (Frank et al., 2012). These models should represent processes along the continuum of soil, groundwater, and stream. For example, nitrogen (N) is both a critical plant macronutrient needed to achieve high agricultural productivity and a potential source of pollution (McLellan et al., 2018). Within the Chesapeake Bay Watershed (CBW), Ator and Garcia (2016)

estimated that 18% of the N input to the CBW as fertilizer, biological fixation, and deposition is delivered to tidal waters or stored in the stream, with 19% harvested, and 45% lost as denitrification. The majority of N losses occur due to a large mismatch between N extraction in harvest and N application as fertilizer (McLellan et al., 2018; Woodbury et al., 2018). Additionally, high N losses as denitrification suggest potentially high and unreported losses of N₂O if denitrification is incomplete (Saha et al., 2021), a process that is challenging to simulate at any scale (Boyer et al., 2006). Opportunities exist therefore to reduce N losses through cost-effective and environmentally friendly means, with robust modeling and diagnostic tools playing a significant role in leveraging these opportunities.

The conceptualization, development and evaluation of spatially-distributed models (e.g., PALMS, PALM-Scot, SWAT-MODFLOW, and CS-MB) have primarily focused on hydrology (e.g., Kim et al., 2008; Molling et al., 2005), or crop yield and hydrology (e.g., Booker et al., 2015; Ward et al., 2018). A comprehensive evaluation of spatially-distributed models encompassing multi-state observations of hydrology, crop yield, and water quality has not been reported. Furthermore, the potential of spatially-distributed agroecosystem models for agroecosystem design has yet to be thoroughly examined.

The objectives of this paper are to present Cycles-L, a coupled agroecosystem hydrologic modeling system, and to demonstrate its application through a case study conducted at the WE-38 agricultural watershed in Pennsylvania. This watershed is nested in the larger watershed of the Mahantango Creek. The availability of long-term discharge and water quality records, together with the surveys of crop rotations, make WE-38 an ideal site for testing Cycles-L. Our evaluation focuses on comparing simulated water discharge, stream NO₃⁻-N discharge and concentration, and crop yield with observations and county-level surveys. This assessment highlights the accuracy and practicality of Cycles-L for landscape level analysis. Additionally, we conduct virtual experiments by comparing a 1-D version of Cycles with Cycles-L, and by replacing annual crops with switchgrass (*Panicum virgatum* L.) to assess trade-offs between crop production, N losses, and water quality. These experiments exemplify Cycles-L's capability in facilitating agroecosystem design.

2. Cycles-L Components Description

2.1. Flux-PIHM

Flux-PIHM is a high-resolution, spatially-distributed land surface hydrologic model that integrates the Penn State Integrated Hydrologic Model (PIHM; Qu & Duffy, 2007; Bhatt et al., 2014) and the Noah land surface model (LSM) component (F. Chen & Dudhia, 2001; Ek et al., 2003). Flux-PIHM simulates 3-D soil, groundwater, and river hydrology, along with the surface energy balance, representing the variability in land surface and hydrological processes due to soil, landcover, and topographic heterogeneity (Shi et al., 2015). Flux-PIHM is the core of other terrestrial biogeochemistry (Shi et al., 2018; Zhi et al., 2022) and reactive transport models (Bao et al., 2017).

In Flux-PIHM, the land surface is decomposed into unstructured triangular grids for optimal representation of local heterogeneities in topography, soil, and land cover, as well as river channels, and watershed boundaries. River channels are represented by rectangular elements (Tarboton et al., 1991). Water transport between soil, groundwater, and river follows PIHM (Qu & Duffy, 2007). PIHM uses de Saint-Venant (1871) equations to compute channel (1-D) and surface (2-D) water flow. Infiltration at the air-soil interface is calculated using the properties of the top 10 cm of soil following Darcy's law. In the subsurface, the triangular volume is divided into water saturated and unsaturated zones. Water transport in the unsaturated zone only occurs vertically. In the saturated zone, groundwater flow is horizontal with dynamic coupling to the unsaturated zone across the water table following Darcy's law. Unsaturated and saturated zone storages are calculated as:

$$\Theta_s \frac{dh_u}{dt} = q_I - q_R - \eta_u(E_{dir} + E_t), \quad (1a)$$

$$\Theta_s \frac{dh_g}{dt} = q_R - (1 - \eta_u)(E_{dir} + E_t) + \sum_j q_j, \quad (1b)$$

where h_u and h_g are unsaturated and saturated storage depths (m), Θ_s is the soil porosity (m³ m⁻³), q_I is the infiltration (m s⁻¹), q_R is the recharge (m s⁻¹), that is, the flux between unsaturated and saturated zone, E_{dir} is the

evaporation from soil ($m\ s^{-1}$), E_t is the canopy transpiration ($m\ s^{-1}$), and q_j is the normalized (by grid area) lateral water flow at the subsurface between grid i and its neighbors at edges js ($m\ s^{-1}$). The variable η_u represents the fraction of evapotranspiration extracted from the unsaturated zone, thus $(1 - \eta_u)$ is the fraction from the saturated zone.

The hydrologic equations at each model grid are discretized to ordinary differential equations (ODEs), which are assembled within the boundaries of the domain and solved simultaneously using the CVODE ODE solver (Hindmarsh et al., 2005).

The land surface component of Flux-PIHM is adapted from the Noah LSM (F. Chen & Dudhia, 2001; Ek et al., 2003), and is coupled to PIHM by exchanging water table depth, infiltration rate, water table position, net precipitation rate, and evapotranspiration rate between the two components. The land surface component simulates surface energy balance, snow melt, interception, and throughfall. Surface energy balance in Flux-PIHM is calculated as:

$$(1 - A)S\downarrow + \epsilon_L L\downarrow - \epsilon_L \sigma T_{\text{sf}}^4 = G + H + \lambda E, \quad (2)$$

where A is the surface albedo (dimensionless), $S\downarrow$ is the downward solar radiation ($W\ m^{-2}$), ϵ_L is the surface emissivity (dimensionless), $L\downarrow$ is the downward longwave radiation ($W\ m^{-2}$), $\sigma = 5.67 \times 10^{-8}\ W\ m^2\ K^{-4}$ is the Stefan-Boltzmann constant, T_{sf} is the surface skin temperature (K), and G , H , and λE are ground, sensible, and latent heat fluxes ($W\ m^{-2}$), respectively. The total evapotranspiration E is the sum of evaporation from soil, evaporation from canopy water storage (E_c) and canopy transpiration:

$$E = E_{\text{dir}} + E_c + E_t. \quad (3)$$

In the land surface component, the subsurface is divided into layers with fixed thickness. By default, the soil layer thickness increases from 0.11 m for the first layer to 0.38 m for the 10th layer (Shi et al., 2015). The number of soil layers can be reduced, and the thickness of the deepest layer can be adjusted to match the depth to bedrock. PIHM simulates infiltration rate, lateral subsurface flow rate, and position of water table for all model grids. These variables are used as boundary conditions by the LSM to calculate transport within the unsaturated zone using Richards equation. A recent development is adding a topographic solar radiation module to Flux-PIHM (Shi et al., 2018). Flux-PIHM is now the core landscape hydrology model for multiple modeling systems. Detailed descriptions of PIHM and Flux-PIHM are provided by Qu and Duffy (2007), and Shi et al. (2013); Shi et al. (2014, 2018).

2.2. Cycles

Cycles is a one-dimensional process-based multi-year and multi-species agroecosystem model (Kemanian et al., 2022). Cycles evolved from C-Farm (Kemanian & Stöckle, 2010) and shares biophysical modules with CropSyst (Stöckle et al., 2014). Cycles simulates the water and energy balance, the coupled cycling of carbon (C) and N, and plant growth at daily time steps. Evapotranspiration is calculated based on the Penman-Monteith equation. Transpiration is modulated by the evaporative demands, soil water potential, crop root distribution and plant hydraulic properties (Campbell, 1985). Plant development is determined by thermal time, and plant growth is based on solar radiation interception (light limited) or the realized transpiration (water limited) based on stomatal optimization theory (Cowan, 1978, 1982; Katul et al., 2009; Kemanian et al., 2005). Soil organic C and N cycling are based on saturation theory (Kemanian & Stöckle, 2010; Pravia et al., 2019). The model can simulate a wide range of perturbations of biogeochemical processes caused by management practices such as tillage, irrigation, organic and inorganic nutrient additions, annual and perennial crop selections, crop harvests as grain or forages, polycultures, relay cropping, and grazing. Cycles can simulate an unlimited number of plant species as specified by the user.

2.3. Cycles-L

Cycles-L (Figure 1) takes the landscape and hydrology structure from Flux-PIHM and most agroecosystem processes from Cycles. The surface energy balance and soil hydrology are simulated as in Flux-PIHM, except for plant water uptake and the water balance of surface plant residues, which use Cycles' algorithms. Specifically, plant water uptake simulated with Cycles replaces E_t from Flux-PIHM in Equations 1a, 1b and 3, and

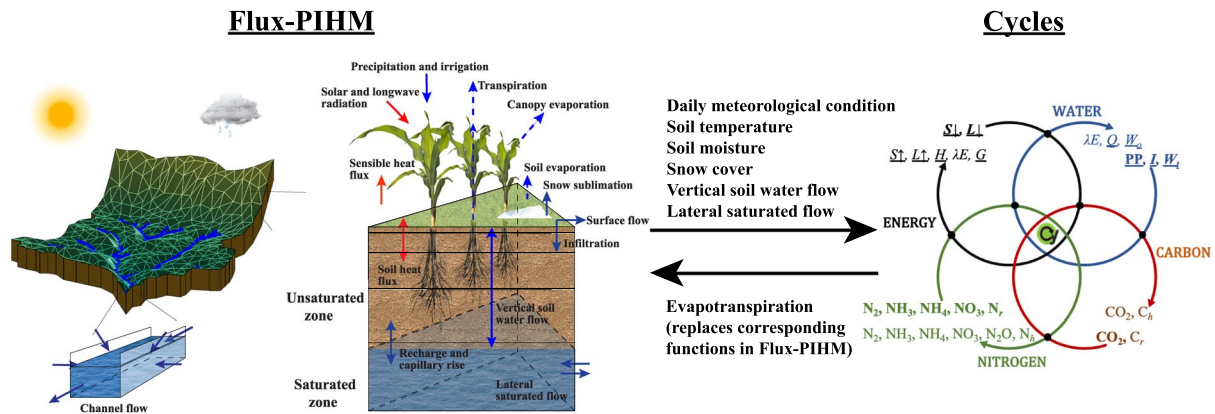


Figure 1. Schematic illustration of land surface and hydrologic processes simulated by Flux-PIHM; energy, water, carbon (C) and nitrogen (N) cycles simulated by Cycles with fluxes in and out for each component; and the coupling between Flux-PIHM and Cycles. For Cycles, the nodes at the arrows' intersections represent interactions between cycles; $S \downarrow$ and $L \downarrow$ are incoming shortwave and longwave radiation, $S \uparrow$ and $L \uparrow$ are outgoing shortwave and longwave radiation, H , λE , and G are sensible, latent, and ground heat fluxes, PP is precipitation, I is irrigation, W_c is capillary rise, Q is runoff, W_o is soil percolation or lateral flow, C_r and N_r are C and N changes caused by soil amendments, and C_h and N_h are harvested C and N. Carbon enters the system primarily through photosynthesis and is mostly lost through respiration and grain and forage harvest. Nitrogen enters through biological N fixation, deposition, and fertilization, and is lost in gaseous forms (N_2 , NO , N_2O , NH_3) and as dissolved NO_3 and NH_4 . When coupled, the processes represented by dashed arrows in Flux-PIHM are simulated by Cycles, and the fluxes with underlines in Cycles are calculated by Flux-PIHM.

Equation 3 is also expanded by adding the evaporation from residue (E_r) to the total evapotranspiration. Flux-PIHM simulated soil moisture, soil temperature and snow cover will inform Cycles, to modulate agroecosystem processes. Hydrologic processes are simulated with a sub-daily time step (usually $\sim 10^0$ min, dynamic). Following Cycles' structure, each soil layer has texture- and organic matter-dependent hydraulic properties. When activating landscape hydrology, the properties of the soil profile are averaged preserving total soil mass and porosity to allow solving for vertical and lateral fluxes using Flux-PIHM. Biogeochemical processes are simulated with a daily time step independently for each soil layer. Tillage operations allow mixing all components of the soil layers affected by tillage. The one-dimensional Cycles model is integrated into every Flux-PIHM model grid. Therefore, each model grid can be assigned a unique land cover or crop rotation.

At the beginning of each simulation day, land surface processes are calculated first using the Noah LSM, with Noah LSM evapotranspiration functions replaced by the corresponding Cycles functions. Thereafter, management operations are implemented and vegetation, residue, and soil C and N processes are simulated using Cycles. The inputs are the daily meteorological conditions, soil temperature, soil moisture, and snow cover informed by Flux-PIHM. Evapotranspiration rate and N fluxes are passed from Cycles to Flux-PIHM as source/sink terms. Then, the transport of water and N for the entire domain is resolved using Flux-PIHM at sub-daily time steps.

A solute transport module is used to simulate subsurface nutrient transport. This model is the same as the subsurface transport in Flux-PIHM-BGC (Shi et al., 2018), and is used to calculate total solute flowing in or out of a model grid i :

$$V \frac{d}{dt}(\Theta C) = \sum_j (-Q_j C_{ij}) + F, \quad (4)$$

where V is the subsurface prism volume of grid i (m^3), C is the subsurface mineral N concentration ($kg\ m^{-3}$), Θ is the volumetric soil water content ($m^3\ m^{-3}$), Q_j is the lateral water flow at the subsurface between grid i and its neighbor at edge j ($m^3\ s^{-1}$), and F is a source/sink term of the corresponding solute ($kg\ s^{-1}$). In Cycles-L, the source/sink terms for mineral N are:

$$\begin{aligned} \frac{d}{dt} NO_3^- - N &= NO_3^- - N_f + NO_3^- - N_d + NO_3^- - N_{nit} + NO_3^- - N_{imm} \\ &- NO_3^- - N_{dnt} - NO_3^- - N_{pup} - NO_3^- - N_l - NO_3^- - N_r \end{aligned} \quad (5a)$$

and

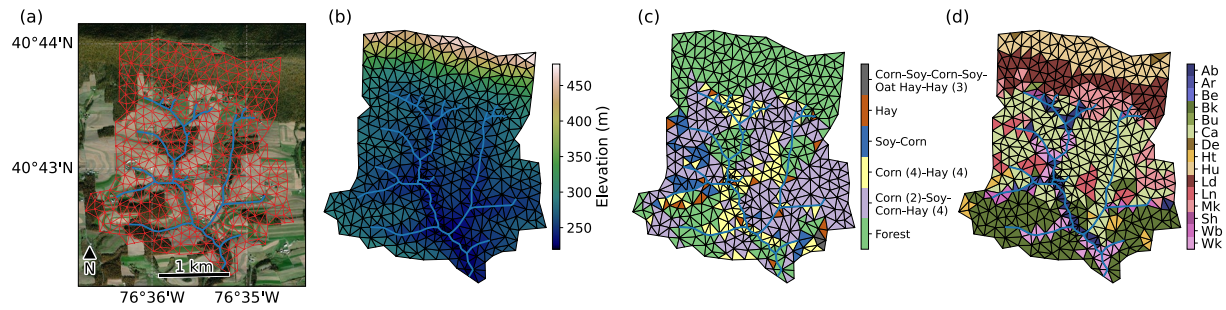


Figure 2. (a) WE-38 model domain projected onto an aerial photograph of the watershed. The red triangles represent the model grids and the blue lines represent river segments. (b) Surface elevation map of the WE-38 model domain. (c) Land use and crop rotations in the WE-38 model grids. (d) SSURGO soil map projected onto WE-38 model grids, with each color representing one unique soil type. The soil series are Albrights silt loam (Ab), Alvira silt loam (Ar), Bedington silt loam (Be), Berks channery silt loam (Bk), Buchanan channery loam (Bu), Calvin-Klinesville shaly silt loams (Ca), Dekalb very channery sandy loam (De), Hartleton channery silt loam (Ht), Hazleton and Clymer extremely stony sandy loams (Hu), Laidig and Meckesville extremely stony soils (Ld), Leck kill shaly silt loam (Ln), Meckesville silt loam (Mk), Sheldahl silt loam (Sh), Watson silt loam (Wb), and Weikert and Klinesville shaly silt loams (Wk).

$$\frac{d}{dt} \text{NH}_4^+ \text{-N} = \text{NH}_4^+ \text{-N}_f + \text{NH}_4^+ \text{-N}_d + \text{NH}_4^+ \text{-N}_{\text{min}} - \text{NH}_4^+ \text{-N}_{\text{nit}} - \text{NH}_4^+ \text{-N}_{\text{imm}} - \text{NH}_4^+ \text{-N}_{\text{pup}} - \text{NH}_3 \text{-N}_{\text{vol}} - \text{NH}_4^+ \text{-N}_l - \text{NH}_4^+ \text{-N}_r \quad (5b)$$

where subscript f is for fertilizer, d for deposition, nit for nitrification, imm for microbial immobilization or microbial uptake, pup for plant uptake, dnit for denitrification, l for leaching or percolation, r for runoff, min for mineralization of organic compounds with N (many), and vol for volatilization as $\text{NH}_3\text{-N}$. Note that $\text{NO}_3^- \text{-N}_{\text{nit}}$ and $\text{NH}_4^+ \text{-N}_{\text{nit}}$ are the same, and NH_4^+ and NO_3^- are just N species identifiers. If the net water flow from a grid is outward (net efflux from grid i to grid j) then the mineral N concentration (C_{ij}) of the water flow (Q_j) is that of grid i : $C_{ij} = C_i$; otherwise, $C_{ij} = C_j$. In Flux-PIHM, horizontal water flow is restricted to the saturated zone. But this horizontal flow is calibrated to include the representation of lateral perched flow above unsaturated layers; that flow can drag mineral N (M. R. Williams et al., 2015) or other solutes. This is difficult to predict because it depends on the mixing between water flowing through macropores and water in the non-macropore soil matrix, and the distribution of mineral N. To account empirically for that mixing, we tentatively assigned a weighting function that allows for mineral N transport from unsaturated layers. The weighting function is $\frac{K_r}{D-d_z}$, where K_r is the relative hydraulic conductivity (hydraulic conductivity divided by saturated hydraulic conductivity), D is the total soil depth, and d_z is the depth of the corresponding soil layer. This function is applied to all soil layers when calculating the average concentration of soil mineral N, to emulate the horizontal transport of mineral N in the shallower depths with higher hydraulic conductivities. Due to the very low hydraulic conductivity of dry soil layers, their contribution to mineral N transport is negligible.

3. Site and Data

3.1. Description of the WE-38 Watershed

The WE-38 watershed is a 7.3 km² first-order watershed within the Mahantango Creek Watershed in Pennsylvania's Northumberland county (Figure 2a). Elevation ranges from 503 m at the northernmost ridge to about 214 m near the southern outlet. The land cover comprises cultivated land (55%), followed by forests (40%), pasture (3%), and developed area (2%). The watershed contains more than 300 farm fields. Surveys and interviews were used to obtain field-specific operations (Veith et al., 2015) that documented crop species, planting and harvesting dates, tillage tools and operation dates, and synthetic fertilizer and animal manure application rates and dates. The watershed has been the focus of rigorous research on agricultural management and monitoring of water quality (Bryant et al., 2011; Buda et al., 2011; Church et al., 2011; Lu et al., 2015; Pionke et al., 2000; Veith et al., 2015), and long-term discharge and water quality measurements, including $\text{NO}_3^- \text{-N}$ and $\text{NH}_4^+ \text{-N}$, are publicly available.

3.2. Model Domain and Setup

The Cycles-L WE-38 model physical domain consists of a stream network represented by 114 segments (average length of 98 m) and land represented by 883 triangular grids (average area of 0.83 ha), of which 522 are

Table 1
Field Operations for Crops in the Rotation

Operation	Day of year	Fertilizer mass (kg ha ⁻¹)	Fertilizer N-P-K
Corn			
Manure fertilizer	100	3,500	03-01-00
Tillage moldboard	101		
Tillage disking	102		
Planting	121		
Fertilization	121	100	10-20-20
Fertilization	152	100	33-00-00
Harvest and kill crop			
Soybean			
Manure fertilizer	100	1,875	03-01-00
Tillage disking	102		
Planting	121		
Harvest and kill			
Hay (oats)			
Tillage chisel + cultivator	92		
Planting	97		
Fertilization	97	300	03-15-48
Fertilization	166	100	33-00-00
Harvest and kill	219		
Hay (alfalfa + orchardgrass)			
Tillage (year 1)	101		
Planting (year 1)	105		
Fertilization manure (year 1)	100	3,500	03-01-00
Fertilization (year 1)	259	100	02-11-45
Clipping and haying (4 times)	Various		
Fertilization all years (4 times)	Various	100	02-11-45
Kill (year 4)	303		

Note. The N-P-K refers to the proportion of N, P, and K in the dry mass. For manure, 25% of N is added as NH₄⁺ and 75% as organic N with C:N ratio of 14. For hay, fertilization follows after a clipping and haying event.

cropland (Figure 2). The watershed stream network was mapped using the Terrain Analysis Using Digital Elevation Models tool (TauDEM; Tarboton et al., 2009; Tarboton, 2015) on a digital elevation model obtained from light detection and ranging (lidar) data and color orthophotography at horizontal and vertical resolutions of 0.5 and 0.15 m, respectively (Bryant et al., 2011). Afterward, the stream network was updated by overlapping the TauDEM analysis output with a georeferenced orthomosaic of the watershed obtained from the Pennsylvania Spatial Data Access (PASDA, 2022).

To represent field operations, we converted the database used for WE-38 in Hirt et al. (2020) to Cycles-L inputs. This database aggregates field operations history by crop in the rotation. These rotations and associated field operations were projected on the Cycles-L WE-38 model domain (Figure 2c). Model grids were assigned to one of six land uses: deciduous forest, a corn (2 years)-soybean-corn-hay (4 years) rotation, a corn (4 years)-hay (4 years) rotation, a soybean-corn rotation, a hay rotation, and a corn-soybean-corn-soybean-oat hay-hay (3 years) rotation. Hay was simulated as a mixture of 1/3 alfalfa and 2/3 orchardgrass. Deciduous forest is the most common land use type, while the corn (2 years)-soybean-corn-hay (4 years) rotation is the most common crop rotation. The operations for each crop are listed in Table 1.

To prevent an unrealistic rotation synchrony in grids with the same rotation, we randomly assigned a different starting point in the rotation to each grid within the assigned rotation. For example, for the model grids with the soybean-corn rotation, we randomly assigned half of those grids to start with soybean, and the other half to start with corn.

The soil texture, organic matter, and bulk density (by layer) were extracted from the SSURGO database projected to the model domain (Figure 2d); 15 unique soil series were identified for the watershed. Soil hydraulic parameters of the 15 soil series were calculated using the pedotransfer functions developed by Wösten et al. (1999). The a priori parameter values are presented in Table 2. The meteorological forcing (precipitation, air temperature, humidity, wind speed, downward solar radiation, downward longwave radiation, and air pressure) were obtained from the North American Land Data Assimilation System Phase 2 (NLDAS-2; Xia et al., 2012) forcing data, which provides data at hourly time-step and is suitable for hydrologic simulations.

For model testing, annual crop yields were downloaded from the United States Department of Agriculture (USDA) National Agricultural Statistics Service at county level (Northumberland county) and compared with both Cycles 1-D and Cycles-L for the entire watershed.

3.3. Model Spin-Up and Calibration

The simulation period was 16 years from 0000 UTC 1 January 2000 to 0000 UTC 1 January 2016. To stabilize hydrological and biogeochemical soil properties, the model was spun-up in two steps: one for hydrological variables and another one for agroecosystem variables. Considering the higher computational cost of running Cycles-L compared to Flux-PIHM, we first ran Flux-PIHM for land surface hydrological parameter calibration and hydrological state spin-up. When doing so, the forest was simulated as the deciduous forest NLCD land cover type, the hay rotation was simulated as the pasture/hay land cover type, and all other crop rotations were simulated as the cultivated crop land cover type. The leaf area index (LAI) forcing was prescribed monthly via a climatological LAI that depends on land cover type. Flux-PIHM hydrologic and land surface parameters were manually calibrated using the observed discharge data from 2000 to 2011. Model parameters that affect horizontal water flow and key parameters identified from Flux-PIHM sensitivity analyses (Shi et al., 2014; Xiao

Table 2
Soil Parameters and the Global Calibration Coefficients Used for the WE-38 Watershed Domain

Soil type	K_{inf}	K_V	K_H	Θ_s	Θ_r	α	n
Albrights silt loam	0.26	0.22	2.15	0.44	0.05	2.92	1.16
Alvira silt loam	0.12	0.13	1.30	0.39	0.05	1.85	1.15
Bedington silt loam	0.30	0.26	2.60	0.47	0.05	2.72	1.16
Berks channery silt loam B	0.52	0.83	8.34	0.54	0.05	1.81	1.28
Berks channery silt loam C	0.55	0.86	8.62	0.54	0.05	1.84	1.28
Berks channery silt loam D	0.57	0.87	8.67	0.54	0.05	1.78	1.29
Buchanan channery loam	0.66	0.37	3.71	0.47	0.05	4.22	1.18
Calvin-Klinesville shaly silt loams	0.36	0.43	4.32	0.49	0.05	2.47	1.21
Dekalb very channery sandy loam	1.79	0.98	9.84	0.51	0.05	3.63	1.30
Hartleton channery silt loam	0.27	0.28	2.79	0.47	0.05	2.54	1.17
Hazleton and Clymer extremely stony sandy loams	1.91	0.92	9.22	0.48	0.05	4.26	1.35
Laidig and Meckesville extremely stony soils	0.34	0.20	2.02	0.42	0.05	3.90	1.16
Leck kill shaly silt loam	0.23	0.28	2.79	0.45	0.05	2.46	1.19
Meckesville silt loam	0.19	0.20	2.05	0.45	0.05	2.32	1.16
Shelmadine silt loam	0.15	0.15	1.48	0.40	0.05	2.29	1.16
Watson silt loam	0.22	0.20	2.05	0.43	0.05	2.65	1.16
Weikert and Klinesville shaly silt loams	0.70	0.85	8.46	0.57	0.05	1.68	1.24
Global calibration coefficient (dimensionless)	1.0	4.0	5.0	0.75	0.75	1.0	1.25

Note. The soil parameters are saturated infiltration hydraulic conductivity (K_{inf} , m d⁻¹), vertical saturated hydraulic conductivity (K_v , m d⁻¹), horizontal saturated hydraulic conductivity (K_h , m d⁻¹), saturation soil porosity and residual porosity (Θ_s and Θ_r , m³ m⁻³), and van Genuchten α (m⁻¹) and n (–).

et al., 2019) were adjusted, including vertical and horizontal saturated hydraulic conductivities, vertical and horizontal saturated macropore hydraulic conductivities, macropore depth, soil porosity, van Genuchten parameters, and canopy stomatal conductance. In the calibration process, we first adjusted the horizontal hydraulic conductivities and macropore depth parameters by calibrating to the base flow recession curves (Jepsen et al., 2016; Shi et al., 2014). Then the other parameters were adjusted by calibrating to the peak discharge rates. The single global calibration multiplier method (Pokhrel & Gupta, 2010; Wallner et al., 2012) was adopted for calibration. A global calibration coefficient is a scalar multiplier applied to the corresponding soil related parameter for all soil types. The global calibration multiplier method significantly reduces the dimension of parameter space and preserves the spatial distribution of soil parameters. The calibration coefficients (multipliers) are presented in Table 2. After calibration, land surface and hydrological states were spun up by recycling the meteorological forcing. Hydrological states are considered steady when the change of watershed average groundwater storage is lower than 1 cm between the beginning and end of a simulation cycle. Steady state condition was reached in 32 years, which required recycling the meteorological forcing twice.

The land surface hydrological state variables after the spin-up were used to initialize the Cycles-L spin-up process. The Cycles-L model was run repeatedly by recycling the 16-year meteorological forcing and prescribed farm operations until the change of soil profile organic carbon was lower than 0.01 Mg ha⁻¹. Cycles-L reached steady state conditions after 11 simulation cycles, that is, 167 simulation years.

We calibrated the crop model using the USDA-NASS survey corn yield by adjusting crop ecophysiological parameters that are site-dependent (rooting depth) and two related parameters that regulate growth potential, the radiation use efficiency (g of biomass accrued per MJ of radiation intercepted) and transpiration use efficiency (g of biomass accrued per kg of water transpired). The last two parameters were reduced to 2/3 of their default values, to represent in a simplified way limitations to growth not accounted for in the input data (shallower soils or compacted layers) or in the model (deficient soil exploration by roots due to rocks); the watershed contains spots with high rock content (Saha et al., 2017). Overestimating yields can severely alter outputs mostly by increasing nutrient extraction in harvested grain or forage.

Mismatches between fertilizer application rates obtained in field surveys and those needed to match crop yield and other variables have been previously reported (USDA-NRCS, 2012, p. 30). We thus ran exploratory Cycles-L simulations with arbitrary N input increases of 25% and 50% over the survey data (hereafter, Cycles-L 1.25× N and Cycles-L 1.5× N) to potentially compensate for underreported fertilizer applications.

3.4. Virtual Experiment Setup

To demonstrate the capability of Cycles-L in agroecosystem design, we ran four additional Cycles-L simulations at WE-38, replacing parts of the cropland with switchgrass. This strategy has been proposed to reduce N loads to the Chesapeake Bay (Woodbury et al., 2018), due to the properties of switchgrass, a fast-growing and perennial plant that produces large amounts of biomass, takes up mineral N efficiently, and can facilitate N removal from the watershed or its recycling through biomass harvest. The proposed strategy is to plant switchgrass in areas in which corn yields are limited by environmental conditions, like high water table or shallow soils, that reduce N uptake by the crop, and therefore leave N available for volatilization, denitrification and leaching. For this purpose, we chose the cropland with the corn (2 years)-soybean-corn-hay (4 years) rotation and the corn (4 years)-hay (4 years) rotation, because both rotations have high fertilizer input rates (Table 1). As explained below, the 1.25× N simulation was used for this purpose. To select the areas to be planted with switchgrass, we ranked the model grids with these two rotations by their average denitrification rate and defined four new scenarios resulting from combining areas with “high” and “low” denitrification rate with two fertilization strategies. In the high denitrification scenario, we replaced switchgrass for the grain-forage rotation in the 25% of total cropland area that had the highest denitrification rate; in the low denitrification scenario, we replaced about the same amount of cropland area that had the lowest denitrification rate. Switchgrass was planted in the first year, and the aboveground biomass was harvested every year. The two fertilization strategies were the “same N” and the “no synthetic N” strategy. In the same N strategy, all model grids with switchgrass received all the fertilization applications used in the 1.25× N cropland grids (change land use but keep the same N application rate). In the “no synthetic N” strategy, the manure fertilization events were retained and the synthetic fertilization events were removed (change land use and reduce the N application rate).

To assess the magnitude of the effect of using a coupled modeling approach (Cycles-L) compared to an hydrologically uncoupled approach (Cycles 1-D), we run Cycles on all grids as if they were independent land units. All unique combinations of crop rotations and soil types were simulated using Cycles. The simulations were also spun-up until the change of soil profile organic carbon was lower than 0.01 Mg ha⁻¹. Results from all Cycles simulations were averaged for the watershed using grid areas as weights to be compared with Cycles-L.

The design of all Cycles-L and Cycles scenario simulations are presented in Table 3.

4. Results

4.1. Simulation of Stream Discharge

Model simulation results from 2000 to 2015 after spin-up and comparisons with field measurements are presented in Figure 3.

Cycles-L captured the interannual variability of discharge, and accurately predicted the timing of most discharge events. The base flow rate predicted by Cycles-L compared well with observations. The Nash-Sutcliffe coefficient (NSE) of daily discharge for the entire simulation period was 0.55. The NSE, however, varied from year to year, with a maximum of 0.85 in 2005. Discharge from multiple years was also averaged to each day of year to glean within-year patterns of measured and modeled discharge (Figure 3b). The model captured the seasonal wet-dry cycles; the predicted discharge magnitude generally agreed well with observations. Cycles-L slightly overestimated discharge, except for late winter and spring. The average annual discharge predicted by Cycles-L is 0.498 m yr⁻¹, which is about 13% higher than the observed 0.442 m yr⁻¹. The NSE for the predicted multi-year average discharge was 0.68. The Cycles-L 1.25× N and 1.5× N simulations produced almost identical water discharge, and are thus not presented.

Flux-PIHM results were similar but not identical to those of Cycles-L (Figure 3a) because while both models share the same hydrologic component, canopy cover is endogenous in Cycles-L and a forcing in Flux-PIHM. The NSE for Flux-PIHM daily discharge prediction was 0.60, which was slightly higher than Cycles-L (0.55). It should be

Table 3
Experiment Design of All Model Simulations and Simulated and Observed Nitrogen Fluxes and Crop Productions in the WE-38 Watershed

	Observed	Cycles (uncoupled)					Cycles-L						
		1×N	1.25×N	1×N	1.25×N	1.5×N	SG-low same N	SG-high same N	SG-low no syn. N	SG-high no syn. N			
Experiment design	-	-	-	-	-	-	-	-	-	-	-	-	-
Fertilization multiplier	-	1.0	1.25	1.0	1.25	1.50	1.25	1.25	1.25	1.25	1.25	1.25	1.25
Manure fertilizer	-	Yes	Yes	Yes	Yes	Yes	Yes	Yes	Yes	Yes	Yes	Yes	Yes
Synthetic fertilizer	-	Yes	Yes	Yes	Yes	Yes	Yes	Yes	Yes	Yes	Yes	Yes	Yes
Switchgrass	-	-	-	-	-	-	L	H	L	H	L	H	H
N flux (watershed average) (kg ha ⁻¹ yr ⁻¹)	-	-	-	-	-	-	-	-	-	-	-	-	-
Fixation and deposition	-	40.4	36.1	45.0	41.9	38.7	35.2	35.1	35.2	35.1	35.2	35.1	35.1
Fertilization (manure)	-	54.8	68.4	54.8	68.4	82.2	68.4	68.4	68.4	68.4	68.4	68.4	68.4
Fertilization (synthetic)	-	30.2	37.8	30.2	37.8	45.3	37.8	37.8	37.8	37.8	34.0	33.9	33.9
Volatilization	-	6.4	7.3	9.4	10.6	11.8	10.1	10.0	10.1	10.0	10.1	10.0	10.0
Denitrification N ₂	-	4.1	5.4	8.1	10.2	12.6	10.9	11.9	10.9	11.9	10.7	10.8	10.8
Denitrification N ₂ O	-	0.2	0.4	0.3	0.5	0.6	0.5	0.6	0.5	0.6	0.5	0.4	0.4
Nitrification N ₂ O	-	0.5	0.6	0.6	0.6	0.7	0.6	0.6	0.6	0.6	0.6	0.6	0.6
Harvest	-	85.4	91.2	77.3	83.7	89.1	73.2	75.0	73.1	75.0	73.1	74.7	74.7
Discharge	29.0	18.6	27.2	22.7	29.9	38.8	33.8	30.9	30.3	30.9	30.3	28.5	28.5
N flux (cropland average) (kg ha ⁻¹ yr ⁻¹)	-	-	-	-	-	-	-	-	-	-	-	-	-
Fixation and deposition	-	50.5	43.1	51.4	45.7	40.2	34.6	34.4	34.6	34.4	34.6	34.5	34.5
Fertilization (manure)	-	94.7	118.4	94.7	118.4	142.0	118.4	118.4	118.4	118.4	118.4	118.4	118.4
Fertilization (synthetic)	-	52.2	65.3	52.2	65.3	78.3	65.3	65.3	65.3	65.3	58.6	58.5	58.5
Volatilization	-	9.7	11.3	13.8	15.9	18.0	15.1	14.9	15.1	14.9	15.0	14.8	14.8
Denitrification N ₂	-	5.7	7.9	10.7	14.3	18.5	15.5	17.2	15.5	17.2	15.1	15.3	15.3
Denitrification N ₂ O	-	0.3	0.6	0.5	0.8	1.1	0.9	0.9	0.9	0.9	0.8	0.8	0.8
Nitrification N ₂ O	-	0.7	0.8	0.7	0.8	0.9	0.8	0.8	0.8	0.8	0.8	0.8	0.8
Harvest	-	147.7	157.7	133.7	144.8	154.1	126.5	129.7	126.5	129.7	126.5	129.2	129.2
Crop production (Mg yr ⁻¹)	-	-	-	-	-	-	-	-	-	-	-	-	-
Corn	-	1,278	1,278	1,288	1,288	1,288	933	975	932	975	932	975	975
Soybean	-	138	138	123	123	123	98	102	98	102	98	102	102
Hay (alfalfa + orchardgrass)	-	2,047	2,254	1,724	1,947	2,121	1,371	1,442	1,371	1,442	1,371	1,443	1,443
Hay (oats)	-	4	4	3	3	3	3	3	3	3	3	3	3
Switchgrass	-	0	0	0	0	0	995	926	995	926	995	925	925

Note. All crop production are watershed annual total. In the experiment design, L and H represent low denitrification and high denitrification, respectively, which are defined as the grids that have low and high denitrification rates within the corn (2 years)-soybean-corn-hay (4 years) rotation or the corn (4 years)-hay (4 years) rotation locations.

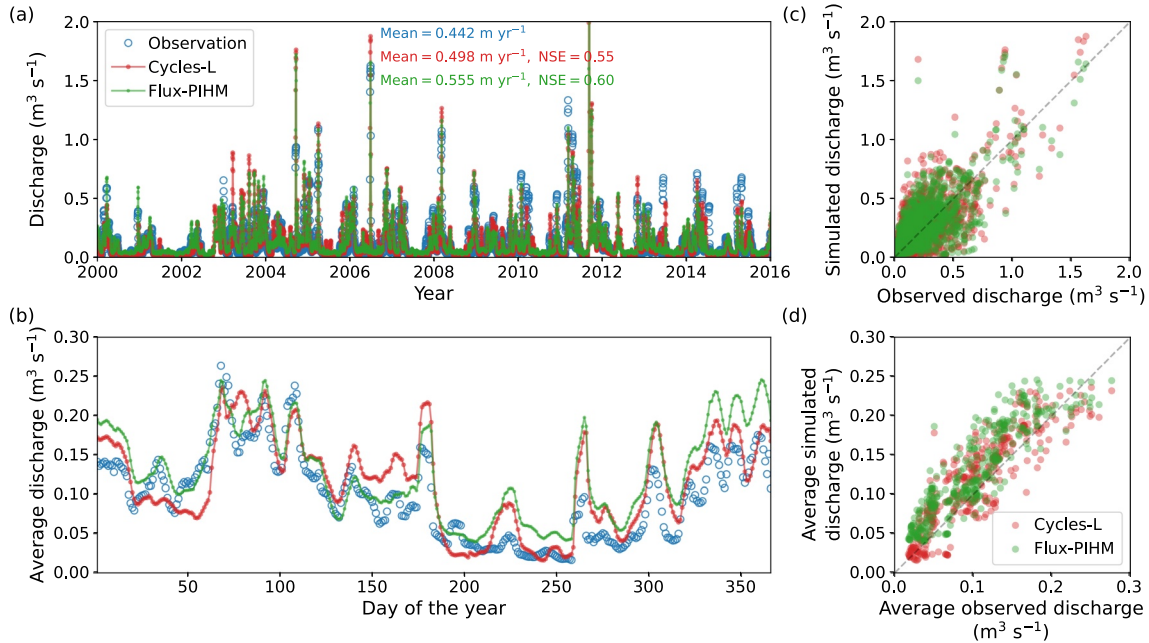


Figure 3. (a) Comparison of daily discharge between observations and outputs from Cycles-L and Flux-PIHM, from 1 January 2000 to 31 December 2015. (b) Comparison of daily discharge when averaged to each day of year. One-to-one comparisons are shown in (c) and (d), respectively.

noted that the land surface and hydrologic parameters in Cycles-L were calibrated by running Flux-PIHM and not recalibrated when applied to Cycles-L, which may cause Flux-PIHM to yield slightly better performance in terms of NSE. However, Flux-PIHM tended to overestimate discharge (0.555 m yr⁻¹, 26% overestimation). Compared to Cycles-L, Flux-PIHM produced higher discharge in spring, and lower discharge in other seasons.

Surface runoff and subsurface drainage of all Cycles simulations were aggregated as a proxy of stream discharge. The average stream discharge estimated by Cycles simulations was 0.602 m yr⁻¹, which is 36% higher than the observed one. The NSE for the Cycles' estimated discharge is -1.96, showing that the aggregated 1-D simulations could not capture the observed daily variations of stream discharge as the lagging effects of storage in groundwater and discharge through groundwater, among other processes, are ignored.

4.2. Simulation of Grain Yield

On average, both Cycles-L and Cycles captured the corn yield variation well (Figure 4), with R^2 of 0.72 for Cycles-L and 0.65 for Cycles, and root mean square errors (RMSEs) of 1.2 Mg ha⁻¹ for both Cycles-L and Cycles. When comparing the first differences of corn yield, which detrend yield increases with time due to

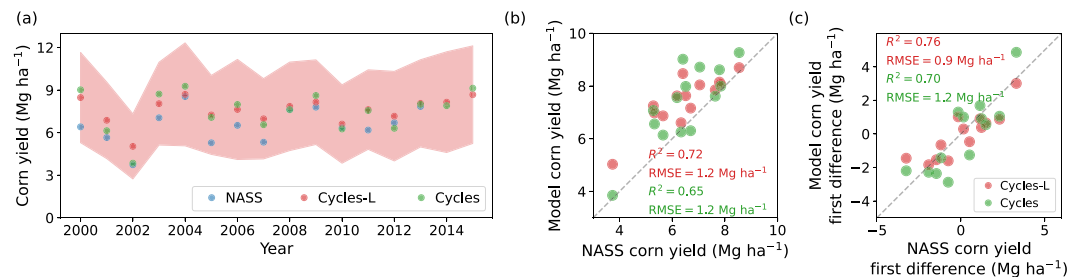


Figure 4. (a) Temporal variation of USDA-NASS survey corn yield and both Cycles-L and Cycles 1-D predicted annual average corn yield from 2000 to 2015. The USDA-NASS survey is for Northumberland County, PA. The shaded area represents the one standard deviation of corn yield as simulated by Cycles-L. (b) Cycles-L and Cycles 1-D predicted annual average corn yield versus USDA-NASS survey annual corn yield. (c) First difference of Cycles-L and Cycles 1-D predicted annual average corn yield versus first difference of USDA-NASS survey annual corn yield.

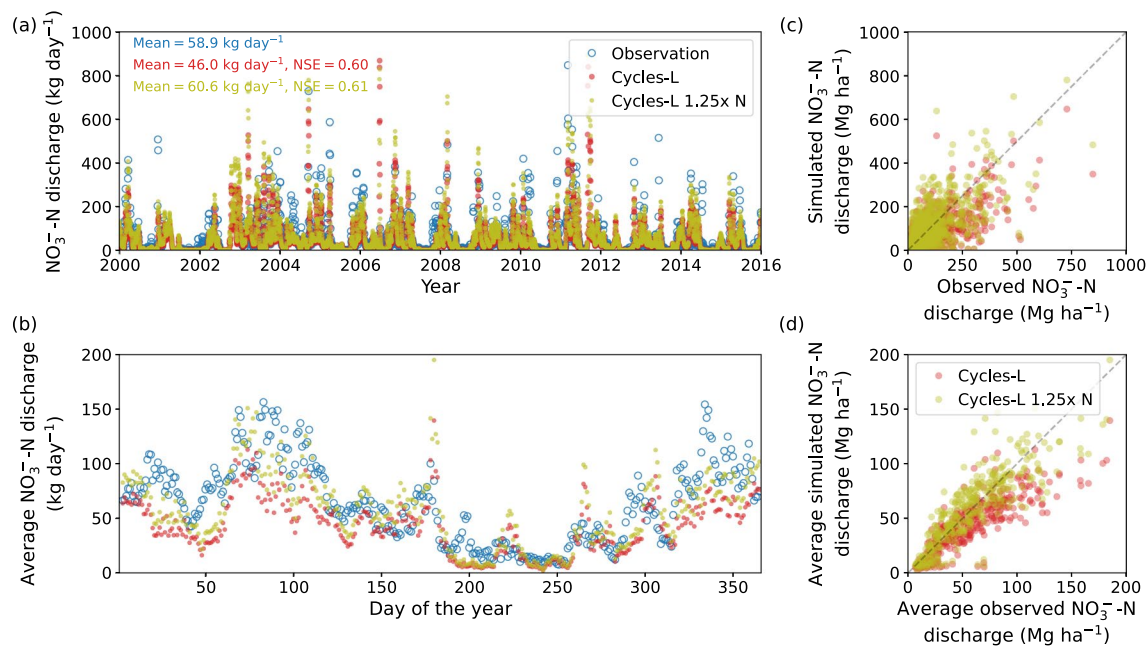


Figure 5. (a) Comparison of daily nitrate-N discharge between the observations and two Cycles-L simulations ($1\times N$ and $1.25\times N$), from 1 Jan 2000 to 31 Dec 2015. (b) Comparison of daily nitrate-N discharge when averaged to each day of year. When averaged to each day of year, a 3-day moving average was applied to both observations and predictions to better reveal the temporal patterns. One-to-one comparisons are shown in (c) and (d), respectively.

technology, the R^2 for Cycles-L increased to 0.76 and that for Cycles increased to 0.70. The shaded area in Figure 4a illustrates the spatial variation of corn grain yield predicted by Cycles-L. The spatial variation of corn yield was larger when yield was higher, and smaller when yield was lower. The standard deviations of corn yield in space varied between 2.3 and 3.6 Mg ha⁻¹. The USDA-NASS survey reported yields were always within the predicted one-standard-deviation (Figure 4a).

4.3. Simulation of Mineral Nitrogen Discharge and Concentration in the Stream

We focused on the N exported at the watershed outlet, where comparisons with measurements allow a reality-bounded assessment of the impact of changing N fertilization rates and other inputs. The temporal patterns of water discharge (Figure 3) and n discharge (Figure 5) are similar, because N discharge is controlled by water discharge. Accordingly and with the inputs from Hirt et al. (2020), the N discharge pattern was correctly simulated by Cycles-L with an NSE of 0.60, but the N mass discharged through the stream was consistently underestimated compared with measurements (Figure 5). The observed and predicted average NO_3^- -N discharge were 57.2 and 45.5 kg day⁻¹, respectively.

Because the stream discharge was slightly overestimated and NO_3^- -N underestimated, the concentration of NO_3^- -N was also underestimated, as was the seasonal variation in NO_3^- -N concentration (Figure 6). The average observed NO_3^- -N concentration in the stream was 5.4 mg L⁻¹, with a pronounced W-shaped seasonal pattern with highs in early summer and in winter, and lows in spring and autumn (Figure 6b). Interannual variability was also noticeable. The simulations consistently underestimated the concentration of NO_3^- -N, on average by about 30%, and significantly underestimated the magnitude of seasonal variations.

NO_3^- -N in discharge predicted by the Cycles-L $1.25\times N$ simulation significantly improved over the default $1\times N$ simulation. Comparing Cycles-L $1\times N$ with Cycles-L $1.25\times N$, the NO_3^- -N discharge changed from 45.5 to 60.0 kg day⁻¹, much closer to the observed discharge of 57.2 kg day⁻¹. The discharge of NO_3^- -N predicted with Cycles-L $1.5\times N$ was higher (+19.7 kg day⁻¹, not shown in the figure) than the observed discharge. Although the $1.25\times N$ simulation underestimated stream NO_3^- -N concentration in early summer and winter, deviations in multi-year average N discharge for this time period were small, because the model's overestimation of water discharge for the same time period (Figure 3b) compensated for deviations in NO_3^- -N concentration. The $1.25\times N$ simulation overestimated NO_3^- -N concentration in 2000 and 2001 and underestimated it in 2003, 2004, and 2005 (Figure 6a). For other years, the predicted NO_3^- -N concentration agreed well with observations, especially for the

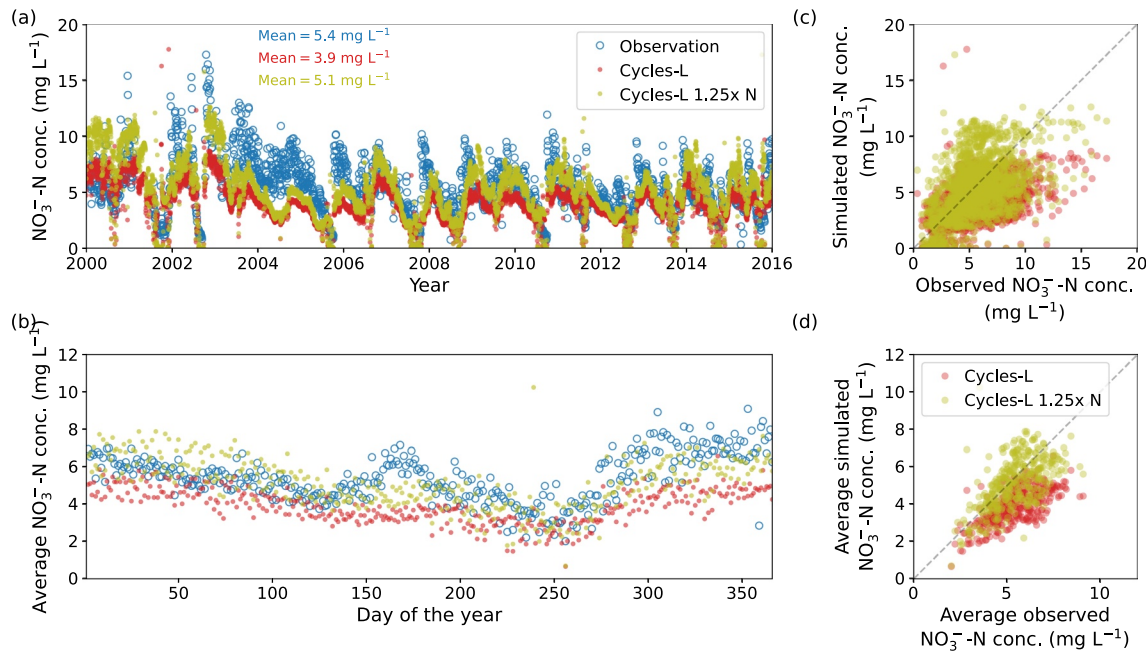


Figure 6. (a) Comparison of daily stream nitrate-N concentrations between observations and two Cycles-L simulations (1× N and 1.25× N), from 1 January 2000 to 31 December 2015. (b) Comparison of daily nitrate-N concentrations when averaged to each day of year. One-to-one comparisons are shown in (c) and (d), respectively.

second half of the simulation (from 2008 to 2016), despite missing some peaks. When averaged to each day of year, the model captured the seasonal variation of NO₃⁻-N concentration very well (Figure 6b).

4.4. Spatial Patterns of Simulated Nitrogen Fluxes

Nitrogen flux predictions of the Cycles-L 1.25× N simulation were used for this analysis, because this simulation best captured the mineral N concentration in the stream. Since the model has been run to steady state, the change of N storage in the system was low. On average, most N removals other than discharge occurred through N harvest, NH₃-N volatilization, and NO₃⁻-N denitrification (Table 3).

Due to the distribution of the cropland and forestland, N inputs had a marked spatial distribution (Figure 7a). Yet, the spatial patterns of N losses were also shaped by topography and soils because they influence hydrology. The spatial pattern of N input was clearly controlled by crop management. Forests and the areas with the hay rotation have low N input because there was no fertilization but only deposition and biological fixation. The spatial pattern of NH₃-N volatilization was highly correlated with the pattern of fertilization. The spatial patterns of denitrification and N₂O emission illustrate the complex interactions between crop management and topography. The forests had a lower denitrification rate (and N₂O emission) compared to areas with crop rotations. For the areas with crop rotations, denitrification rates (and N₂O emission) were higher in headwaters and in some areas of convergent flow or flat terrain near the stream, where soil water content was higher. Nitrogen harvest was largest in areas with a high frequency of corn and soybean.

Fluxes from the Cycles 1.25× N simulation were mapped to corresponding Cycles-L model grids with the same combinations of crop rotations and soil types. While the gridded Cycles 1-D simulations captured the spatial variations of N fluxes caused by different crop rotations and soils, they failed to represent the variations caused by topography (Figure 7b). For example, Cycles-L predicted N flux variations along the topographic gradient in the upland forest, which were not captured by gridded Cycles 1-D predictions. Critically, the hot spots of denitrification and N₂O emission at the stream heads predicted by Cycles-L were also missing in the gridded Cycles 1-D predictions. As a result, the average denitrification rate was almost 2× higher in Cycles-L (Table 3).

4.5. Switchgrass Experiments

Table 3 shows the tradeoff among corn, soybean, hay and switchgrass production, as well as changes in N fluxes and water quality across the simulated scenarios. Reducing the grain crops area reduced, accordingly, grain

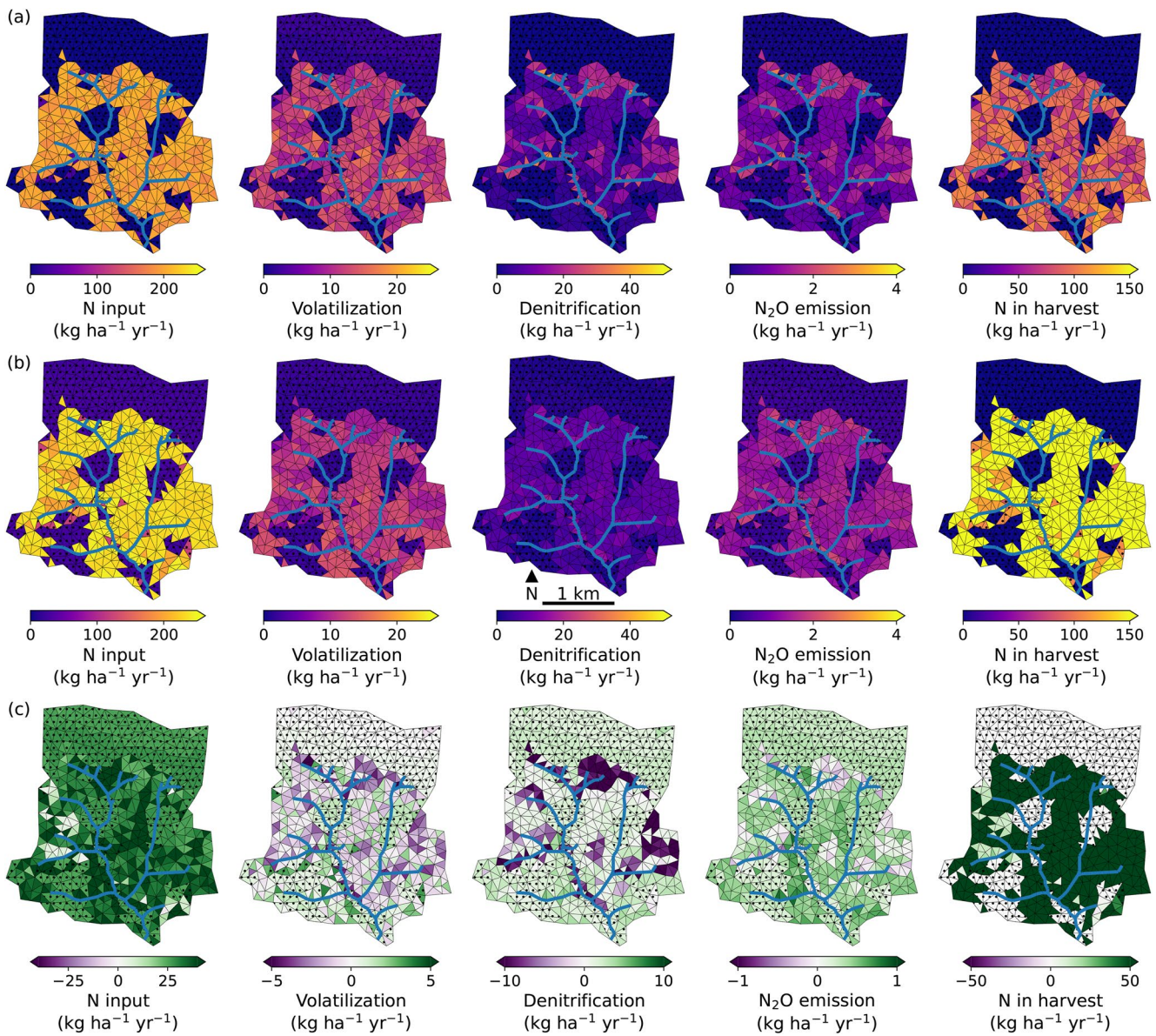


Figure 7. Spatial patterns of nitrogen fluxes (nitrogen input, nitrogen volatilization, denitrification, N_2O emission, and nitrogen in harvest) as estimated by (a) the Cycles-L 1.25 \times N simulation, (b) the Cycles 1-D 1.25 \times N simulation, and (c) the difference between the Cycles 1-D and Cycles-L simulations. For each model grid, the fluxes were averaged over the whole simulation period. For the Cycles 1-D 1.25 \times N simulation, the fluxes were mapped to Cycles-L model grids with the same combinations of crop rotations and soil types. The dotted areas represent the forests and areas with the hay rotation. The blue lines represent river segments.

production. Compared with planting switchgrass in low denitrification areas (Cycles-L SG-low, same N), doing so in high denitrification areas (Cycles-L SG-high, same N) resulted in higher corn production (5%), higher soybean production (4%), higher hay production (5%), and lower nitrogen discharge (Table 3). Planting switchgrass in low denitrification areas, however, produced more switchgrass (about 7%). Removing synthetic N fertilizer from switchgrass but retaining the added manure (Cycles-L SG-high, same N and SG-low, same N) did not reduce switchgrass production. When switchgrass replaced cropland and synthetic N fertilization was reduced, the total N input rate decreased by about $11 \text{ kg ha}^{-1} \text{ yr}^{-1}$ ($18 \text{ kg ha}^{-1} \text{ yr}^{-1}$ if considering only cropland area) with only a $4 \text{ kg ha}^{-1} \text{ yr}^{-1}$ reduction in N fertilizer (the remaining $7 \text{ kg ha}^{-1} \text{ yr}^{-1}$ are due to the reduction in biological N fixation). Thus, N inputs in this watershed are tied to manure disposal in cropland, and replacing 25% of the cropland area with switchgrass reduced N discharge only when the high denitrification areas were considered and by only $1.4 \text{ kg ha}^{-1} \text{ yr}^{-1}$ (compare 28.5 and $29.9 \text{ kg ha}^{-1} \text{ yr}^{-1}$ of N discharge in Table 3), or about 10%–15% of the reduction in N input. When replacing the high denitrification cropland areas with switchgrass, N discharge

was consistently lower over the simulation period, but exhibited a similar temporal pattern; the N harvested was reduced as well. Notably, no reduction in N discharge occurred when low denitrification areas were replaced with switchgrass. Soils in high denitrification areas are wetter and are therefore more sensitive to management practices than change N inputs or land use. The reduction in corn area and to a lesser extent the reduction in soybean area (despite the biological N fixation), remove two important N sinks and reduce N removals through grain harvest.

5. Discussion

5.1. Simulating Hydrology

Cycles-L captured the interannual variability of discharge, and accurately predicted the timing of peak discharge events and base flow rates with minimum manual calibration. This is in line with the high fidelity of the PIHM family models demonstrated for multiple watersheds (Crow et al., 2018; Jepsen et al., 2016; Shi et al., 2013, 2015; Xiao et al., 2019; Zhang et al., 2018; Zheng et al., 2021). Compared with other spatially-distributed agroecosystem hydrological systems, which usually have rectangular model grids, the unstructured triangular grids of Cycles-L provides both computational efficiency and a better representation of local heterogeneity. Unstructured triangular grids capture with ease watershed boundaries, stream networks, and soil and vegetation units (De Schepper et al., 2015; Kumar et al., 2010; Qu & Duffy, 2007). Because grid sizes can differ in Cycles-L, coarser grids can be used in locations with simple topography and homogenous surface properties, while finer grids can be used to capture complex topography and spatial heterogeneity in soil and vegetation. This approach is already suggested by the use of an unstructured mesh to represent tile drains in De Schepper et al. (2015). These features enable applications of models for precision agriculture in ways that are not possible when using 1-D models or are computationally costly when using a structured mesh in 3-D models. In addition, Cycles-L's unique capability to simulate the two-way interaction between stream and riparian zones makes it suitable to evaluate interventions in agricultural areas along floodplains where flooding damage risk is high (Collins et al., 2022).

5.2. Simulating Nitrogen Discharge and Concentration

When using the fertilization rate as prescribed by the survey data (Hirt et al., 2020), the model estimations of water discharge and corn yield agreed well with the observations and survey (Figures 3 and 4), but underestimated the stream NO_3^- -N concentration and NO_3^- -N discharge (Figures 5 and 6). The discharge underestimation amounted to $8.7 \text{ kg ha}^{-1} \text{ yr}^{-1}$ of N (Table 3). Among the possible reasons are that the model overestimated other N losses or that N inputs are underreported. The NO_3^- -N in discharge and NO_3^- -N concentration in the stream predicted by the Cycles-L 1.25× N simulation significantly improved over the default simulation, strongly suggesting that N inputs were underestimated in the surveys.

The Cycles-L 1× N, 1.25× N, and 1.5× N simulations produced almost identical grain crop yield (Table 3) and water discharge, which suggests that grain crop growth was not N limited in WE-38 even when using the 1× fertilization rate. Because crop growth was similar among the three simulations, evapotranspiration and hydrology were comparable, and the three simulations produced similar stream discharge. Increasing the N fertilizer input rate, however, increased hay yield (Table 3) and stream N concentration (Figure 6). It should be noted that adding 50% more N fertilizer did not increase N inputs to the watershed proportionally because of a parallel reduction in N biological fixation of $6.3 \text{ kg ha}^{-1} \text{ yr}^{-1}$ of N (Table 3). If we were to assume that indeed, inputs of N were underestimated in the default simulation (data from Hirt et al., 2020), and that they would scale linearly between our 1.25× N and 1.5× N simulations, we estimate that N inputs obtained through surveys were underestimated by about 30%.

As in Ator and Garcia (2016), denitrification was a significant loss pathway. When spatially averaged over the whole simulation period from 2000 to 2015, denitrification rates generally increased as N input increased (Figure 8), but strong variation existed depending on the rotation and field location. There seems to be a correlation between well drained locations and the location of corn and soybean in the field (Figure 2), likely reflecting producers' choices that facilitate field operations in cash crops (annual cropping in well-drained areas), which may result in lesser than expected N denitrification losses in those fields (Figure 8). However, NO_3^- -N is transported mostly through groundwater, and grids that gain NO_3^- -N through leaching from other grids may have higher denitrification rates than those expected based only on surface N input. Most cropping model grids have

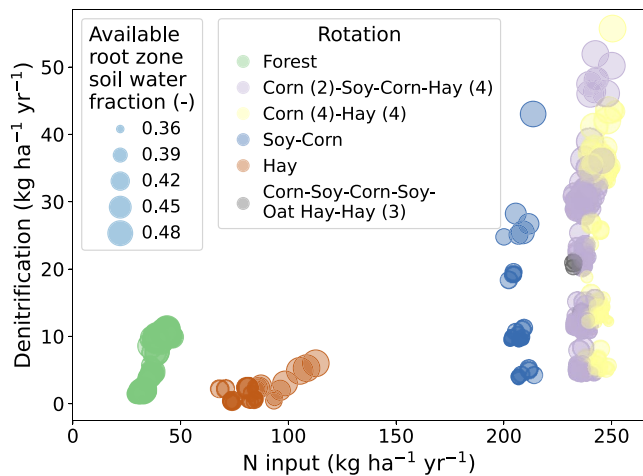


Figure 8. Average denitrification rate versus average nitrogen input as predicted by the Cycles-L 1.25× N simulation. Each circle represents one model grid, averaged over the whole simulation period. The size of the circles represent available root zone soil moisture fraction (fraction between soil wilting point and porosity). The colors represent different land uses/crop rotations.

average N input between 200 and 250 kg ha⁻¹ yr⁻¹, but their simulated denitrification rates varied from around 5 to 60 kg NO₃⁻-N ha⁻¹ yr⁻¹, in large part due to hydrological control of N transport and denitrification. The movement of water alters the spatial distribution of both NO₃⁻-N and oxygen, leading to spatially variable denitrification rates (Groffman et al., 2009; Saha et al., 2017). Denitrification rates within each crop rotation type generally increase with higher soil wetness, as indicated by the size of the circles in Figure 8. This relationship highlights the significant influence of oxygen on denitrification rates in the model: as the air-filled pore space decreases with increasing soil wetness, oxygen replenishment diminishes and oxygen concentration drops thus triggering denitrification. The importance of representing these spatial interactions to model denitrification hot-spots and hot-moments has been previously emphasized by Groffman et al. (2009) and demonstrated through field measurements by Saha et al. (2017). Our modeling framework advances in this direction. However, further improvements are needed to represent denitrification in stream sediments and account for physical features such as the precise location of buried carbon sources (Hill et al., 2014). These improvements will enable us to further refine our understanding and modeling of the spatial distribution of denitrification (Wallace et al., 2020).

5.3. Strength of Cycles-L and Opportunities for Improvement

Owing to its spatially-distributed nature, Cycles-L represents a significant advancement in simulating landscape level processes such as transport of reactive N and other compounds through groundwater and stream water within the watershed domain. It also accounts for the effects of crop rotation, soil type, and weather variations. Moreover, Cycles-L can capture the heterogeneity of agroecosystem processes caused by topography, soil heterogeneity, and management practices. This capability arises from its physically-based hydrologic component, which enables the simulation of horizontal and vertical transport of water and mineral N. Consequently, the framework can integrate other nutrients like soluble phosphorus (McConnell et al., 2020), dissolved organic C (Pabich et al., 2001), and agrochemicals (Hladik & Kolpin, 2015), extending the model applicability.

Comparing Cycles-L predicted N flux patterns with those of 1-D Cycles, the results clearly indicate that Cycles-L can capture the spatial heterogeneity in biogeochemical processes caused by topography in a manner that is not feasible with gridded 1-D model simulations. For example, our results show that while the N harvested in the 1-D uncoupled version of Cycles is 9% (7.5 kg ha⁻¹ yr⁻¹) higher than that with the 3-D Cycles-L, N losses are higher in the latter with 84% and 10% more denitrification and discharge, respectively (+4.9 and + 2.7 kg ha⁻¹ yr⁻¹) (Table 3).

Comparing the average corn yield of Cycles 1-D with the county-level yield averages, a coarse comparison due to the amalgamation of disparate scales, indicates that overall Cycles correctly captures the effect of interannual variations in weather on crop yield. So do other 1-D cropping system models applied in the region (Castaño-Sánchez et al., 2020). Cycles-L did not improve substantially upon these results, although the comparison scope is limited to this small watershed. The simulations with Cycles-L increased the minimum yield most likely due to redistribution of subsurface water in drier years, as most cropland is in the lower portions of the watershed (Figure 3). It is yet to be determined whether employing an even finer resolution (smaller triangles) would render a better representation of hydrology, crop growth, and grain and forage yield. Such finer resolution would also require using dense, grid-specific soil input information. While obtaining such detailed soil information may pose a challenge, yield maps that can be used for testing purposes are already common. Evaluating the effect of a finer resolution in representing specific processes is needed for advancing applications in precision agriculture.

Desirable future improvements include the explicit representation of perched water movement on top of Bt horizons. This would enable lateral water transport above unsaturated soil layers, as opposed to the current approach of lumping this process in the lateral flow calibration parameters. While modeling it explicitly may not improve the overall accuracy of discharge predictions, it may affect mineral N (and other constituents) transport. Similar

considerations apply to modeling water flux through tile drains, with the practical caveat that the location of tile drains is often unknown. When the tile drain network is well mapped it can be explicitly simulated although at the cost of a very dense grid (De Schepper et al., 2015). While the model performs well in its current formulation, future developments should include an explicit representation of tile drains as submerged channels that interact with groundwater.

In Flux-PIHM, macropore flow lumps vertical bypass flow and fast lateral flow of perched water that reaches the stream with minimal mixing with water in the non-saturated soil matrix. This water is then mixed with groundwater. However, in this watershed, measurements have revealed that water can reach streams through ephemeral springs that exfiltrate after lateral transport (Redder et al., 2021). This water can have high concentration of NO_3^- -N, indicating limited mixing with groundwater (M. R. Williams et al., 2015). When measuring in-stream NO_3^- -N concentration, the contribution of water and NO_3^- -N from springs can cause spikier readings in stream NO_3^- -N concentration than when water reaching the stream is mixed with groundwater, as is the case for Flux-PIHM (except for direct runoff). Representing contributions to streams from ephemeral springs can be challenging with lumped parameters, which can help explain the subdued variation in modeled versus measured NO_3^- -N concentration in the stream (Figure 6).

The quality of Cycles-L predictions depends on the model structure as well as the quality of input data. For example, representing large N discharge events requires accurate input of the amount, timing, and composition of N fertilizer and organic amendments. However, the composition of animal manure is highly variable (Griffin et al., 2005), resulting in inherent variance in the addition of N and other nutrients to fields or watersheds via manure. In this study, manure N input represented 42% of the N input in the $1\times$ N scenario (Table 3), and was on average twice as large as the NO_3^- -N watershed discharge. In addition, for the simulations presented here, the prescribed management practices have the same planting dates, tillage dates and practices, and fertilization dates and rates every year, which are approximately correct on average but likely incorrect in any given year of the 16-year simulation period. Therefore using the surveyed management data introduces uncertainty that would reflect in deviations of stream flow and especially NO_3^- -N concentration (Figure 6), regardless of the model algorithms employed. The underestimation of NO_3^- -N discharge when using survey data to represent fertilizer inputs ($1\times$ N) and the improvement through the modeled $1.25\times$ N and $1.5\times$ N scenarios suggest that N inputs through fertilizer were underestimated on average by 30%. Indeed, a mismatch between field survey data on N (and phosphorus) input and that needed to match crop yield and other variables has been reported before (USDA-NRCS, 2012, p. 30).

Cycles-L integrates three models: a hydrologic model (PIHM), a LSM (Noah LSM), and an agroecosystem model (Cycles). The interactions among these components are complex, and even with a conservative approach to model development, the number of parameters involved is large. Previous studies have explored parameter sensitivity in Flux-PIHM (Shi et al., 2014; Xiao et al., 2019), revealing complex interactions among model parameters and between land surface-subsurface processes, which are inherited in Cycles-L. Sensitivity analysis of Cycles-L can help identify critical model parameterization and reveal any potential dependence of model outputs on grid resolution.

Operationally, setting up and running 1-D models, such as a stand alone Cycles 1-D with standardized inputs, are straightforward tasks. Once the soil profile and weather forcing are formatted to conform to requirements, there are no obstacles to running the model. Setting up and running 3-D models present more challenges. While automation has been used in the past to generate input files, grid and stream network for CONUS at the HUC12 level (Leonard & Duffy, 2014), this automation does not guarantee a stable framework to represent hydrology. Often, the grid and stream network setup needs to be streamlined to secure convergence of fluxes and state variables or to avoid resorting to small time steps that slow down execution. However, once a set up is ready, it can be stored, shared, and re-used efficiently to run new scenarios or applications that need to combine measurements and modeling (e.g., Drake et al., 2018).

In summary, Cycles-L can be a valuable tool to understand nutrient cycling in watersheds and to evaluate costly interventions before deployment in the field. Complex interactions among subsurface, land surface, and crops can be explored, gaining valuable insights before committing resources on the ground. Similar outcomes were obtained in prior modeling work using a square grid domain (Beaujouan et al., 2001). Clearly, Cycles-L can be a powerful tool for precision agriculture and precision conservation, serving as a core component of artificial intelligence applications (Gil et al., 2021). The model's spatial and temporal richness, combined with immersive

data visualization tools, can create new opportunities to represent the dynamics of agroecosystems and to develop research, educational, and public engagement tools (C. Wang et al., 2019).

6. Conclusions

Cycles-L is among the first next generation agroecosystem simulation models that are physically based and spatially distributed, thus enabling the representation of landscape processes. The coupling of biogeochemical and hydrologic processes at the catchment scale places this model between 1-D models that simplify terrain and other attributes and global models that connect atmospheric volumes in 3-D but rely on simplified terrestrial models. Cycles-L occupies therefore a unique operational space for research that is relevant to simulate interventions in the landscape.

In the presented test case for Central Pennsylvania, Cycles-L simulated well hydrology, grain crop yield, and N exports in the stream, despite uncertainty in the quality of the input data. Cycles-L retains, therefore, the strengths of Flux-PIHM (Shi et al., 2013) and those of the 1-D Cycles model (Kemanian et al., 2022). Compared to the uncoupled Flux-PIHM (water discharge) and Cycles (crop yield) models, the results with predictions of Cycles-L were either equally good or improved. The model skill at representing the impact of topography, soil heterogeneity, and crop management on N fluxes, both spatially and temporally, expands the scope of in silico agroecosystem analysis to landscape levels.

Further progress will rely on maintaining an equilibrium between the complexity of model algorithms and the simultaneous enhancement in input quality. This will leverage the expanding computing capacity and enable the representation of landscapes with increasing fidelity. We foresee tools such as Cycles-L evolving into indispensable components of the analytical toolkit for both academic and non-academic communities.

Data Availability Statement

The Cycles-L model version 1.0.0 used in this study couples Cycles v1.0.0 with the Flux-PIHM model from the Multi-Modular Penn State Integrated Hydrologic Model (MM-PIHM) v1.0.0. Cycles v1.0.0 source code is preserved at <https://doi.org/10.5281/zenodo.8087162>. MM-PIHM is developed openly at GitHub (<https://github.com/PSUmodeling/MM-PIHM>), available via the MIT license. MM-PIHM v1.0.0 source code is preserved at <https://doi.org/10.5281/zenodo.8087162>. The Cycles-L v1.0.0 executable used for this study is preserved at <https://doi.org/10.5281/zenodo.7942338> (Shi & Kemanian, 2022).

The Cycles-L input data and Jupyter notebooks for data analysis used in the study are available at the GitHub PSUmodeling/Cycles-L-WE38-simulations (<https://github.com/PSUmodeling/Cycles-L-WE38-simulations>) repository via <https://doi.org/10.5281/zenodo.8087264>. Outputs of all Cycles-L simulations are archived at <https://doi.org/10.5281/zenodo.7948951>.

The WE-38 water discharge, nitrate discharge and concentration data were obtained from the USDA data delivery application, STEWARDS. The NLDAS-2 data used in this study were acquired as part of the mission of NASA's Earth Science Division and archived and distributed by the Goddard Earth Sciences (GES) Data and Information Services Center (DISC).

References

- Arnold, J. G., Srinivasan, R., Muttiiah, R. S., & Williams, J. R. (1998). Large area hydrologic modeling and assessment. Part I: Model development. *JAWRA Journal of the American Water Resources Association*, 34(1), 73–89. <https://doi.org/10.1111/j.1752-1688.1998.tb05961.x>
- Ator, S. W., & Garcia, A. M. (2016). Application of SPARROW modeling to understanding contaminant fate and transport from uplands to streams. *Journal of the American Water Resources Association*, 52(3), 685–704. <https://doi.org/10.1111/1752-1688.12419>
- Baker, J. M., Ochsner, T. E., Venterea, R. T., & Griffis, T. J. (2007). Tillage and soil carbon sequestration—What do we really know? *Agriculture, Ecosystems & Environment*, 118(1), 1–5. <https://doi.org/10.1016/j.agee.2006.05.014>
- Bao, C., Li, L., Shi, Y., & Duffy, C. (2017). Understanding watershed hydrogeochemistry: 1. Development of RT-flux-PIHM. *Water Resources Research*, 53(3), 2328–2345. <https://doi.org/10.1002/2016WR018934>
- Basso, B., Bertocco, M., Sartori, L., & Martin, E. C. (2007). Analyzing the effects of climate variability on spatial pattern of yield in a maize–wheat–soybean rotation. *European Journal of Agronomy*, 26(2), 82–91. <https://doi.org/10.1016/j.eja.2006.08.008>
- Batchelor, W. D., Basso, B., & Paz, J. O. (2002). Examples of strategies to analyze spatial and temporal yield variability using crop models. *European Journal of Agronomy*, 18(1), 141–158. [https://doi.org/10.1016/S1161-0301\(02\)00101-6](https://doi.org/10.1016/S1161-0301(02)00101-6)
- Beaujouan, V., Durand, P., & Ruiz, L. (2001). Modelling the effect of the spatial distribution of agricultural practices on nitrogen fluxes in rural catchments. *Ecological Modelling*, 137(1), 93–105. [https://doi.org/10.1016/S0304-3800\(00\)00435-X](https://doi.org/10.1016/S0304-3800(00)00435-X)

Acknowledgments

Funding for this research provided by DoE BETO Grant DE-EE0007088/0000, EPA Grant RD835568, NSF-CNHS Grant ICER-1517823, and USDA-NIFA Award 2012-68005-19703 and 2020-68012-31824, and the College of Agricultural Sciences at Penn State via USA Hatch Appropriations under Project PEN04710 and Accession 1020049.

- Bhatt, G., Kumar, M., & Duffy, C. J. (2014). A tightly coupled GIS and distributed hydrologic modeling framework. *Environmental Modelling & Software*, 62, 70–84. <https://doi.org/10.1016/j.envsoft.2014.08.003>
- Bonilla, C. A., Norman, J. M., & Molling, C. C. (2007). Water erosion estimation in topographically complex landscapes: Model description and first verifications. *Soil Science Society of America Journal*, 71(5), 1524–1537. <https://doi.org/10.2136/sssaj2006.0302>
- Bonilla, C. A., Norman, J. M., Molling, C. C., Karthikeyan, K. G., & Miller, P. S. (2008). Testing a grid-based soil erosion model across topographically complex landscapes. *Soil Science Society of America Journal*, 72(6), 1745–1755. <https://doi.org/10.2136/sssaj2007.0310>
- Booker, J. D., Lascano, R. J., Evett, S. R., & Zartman, R. E. (2014). Evaluation of a landscape-scale approach to cotton modeling. *Agronomy Journal*, 106(6), 2263–2279. <https://doi.org/10.2134/agronj14.0202>
- Booker, J. D., Lascano, R. J., Molling, C. C., Zartman, R. E., & Acosta-Martínez, V. (2015). Temporal and spatial simulation of production-scale irrigated cotton systems. *Precision Agriculture*, 16(6), 630–653. <https://doi.org/10.1007/s11119-015-9397-6>
- Boote, K. J., Jones, J. W., Hoogenboom, G., & White, J. W. (2010). The role of crop systems simulation in agriculture and environment. *International Journal of Agricultural and Environmental Information Systems*, 1(1), 41–54. <https://doi.org/10.4018/jaeis.2010101303>
- Boyer, E. W., Alexander, R. B., Parton, W. J., Li, C., Butterbach-Bahl, K., Donner, S. D., et al. (2006). Modeling denitrification in terrestrial and aquatic ecosystems at regional scales. *Ecological Applications*, 16(6), 2123–2142. [https://doi.org/10.1890/1051-0761\(2006\)016\[2123:MDITAA\]2.0.CO;2](https://doi.org/10.1890/1051-0761(2006)016[2123:MDITAA]2.0.CO;2)
- Bryant, R. B., Veith, T. L., Feyereisen, G. W., Buda, A. R., Church, C. D., Folmar, G. J., et al. (2011). U.S. Department of agriculture agricultural research service Mahantango Creek watershed, Pennsylvania, United States: Physiography and history. *Water Resources Research*, 47(8), W08701. <https://doi.org/10.1029/2010WR010056>
- Buda, A. R., Feyereisen, G. W., Veith, T. L., Folmar, G. J., Bryant, R. B., Church, C. D., et al. (2011). U.S. Department of agriculture agricultural research service Mahantango Creek watershed, Pennsylvania, United States: Long-term stream discharge database. *Water Resources Research*, 47(8), W08703. <https://doi.org/10.1029/2010WR010059>
- Campbell, G. S. (1985). *Soil physics with BASIC: Transport models for soil-plant systems*. Elsevier.
- Castañó-Sánchez, J. P., Rotz, C. A., Karsten, H. D., & Kemanian, A. R. (2020). Elevated atmospheric carbon dioxide effects on maize and alfalfa in the Northeast US: A comparison of model predictions and observed data. *Agricultural and Forest Meteorology*, 291, 108093. <https://doi.org/10.1016/j.agrformet.2020.108093>
- Chen, E., & Mackay, D. (2004). Effects of distribution-based parameter aggregation on a spatially distributed agricultural nonpoint source pollution model. *Journal of Hydrology*, 295(1), 211–224. <https://doi.org/10.1016/j.jhydrol.2004.03.029>
- Chen, F., & Dudhia, J. (2001). Coupling an advanced land surface–hydrology model with the Penn State–NCAR MM5 modeling system. Part I: Model implementation and sensitivity. *Monthly Weather Review*, 129(4), 569–585. [https://doi.org/10.1175/1520-0493\(2001\)129<0569:CAALSH>2.0.CO;2](https://doi.org/10.1175/1520-0493(2001)129<0569:CAALSH>2.0.CO;2)
- Church, C. D., Veith, T. L., Folmar, G. J., Buda, A. R., Feyereisen, G. W., Bryant, R. B., et al. (2011). U.S. Department of agriculture agricultural research service Mahantango Creek watershed, Pennsylvania, United States: Long-term water quality database. *Water Resources Research*, 47(8), W08704. <https://doi.org/10.1029/2010WR010060>
- Collins, E. L., Sanchez, G. M., Terando, A., Stillwell, C. C., Mitasova, H., Sebastian, A., & Meentemeyer, R. K. (2022). Predicting flood damage probability across the conterminous United States. *Environmental Research Letters*, 17(3), 034006. <https://doi.org/10.1088/1748-9326/ac440f>
- Confalonieri, R., Orlando, F., Paleari, L., Stella, T., Gilardelli, C., Movedi, E., et al. (2016). Uncertainty in crop model predictions: What is the role of users? *Environmental Modelling & Software*, 81, 165–173. <https://doi.org/10.1016/j.envsoft.2016.04.009>
- Cowan, I. R. (1978). Stomatal behaviour and environment. In R. D. Preston & H. W. Woolhouse (Eds.), *Advances in botanical research* (Vol. 4, pp. 117–228). Academic Press. [https://doi.org/10.1016/S0065-2296\(08\)60370-5](https://doi.org/10.1016/S0065-2296(08)60370-5)
- Cowan, I. R. (1982). Regulation of water use in relation to carbon gain in higher plants. In O. L. Lange, P. S. Nobel, C. B. Osmond, & H. Ziegler (Eds.), *Physiological plant ecology ii: Water relations and carbon assimilation* (pp. 589–613). Springer. https://doi.org/10.1007/978-3-642-68150-9_18
- Crow, W. T., Milak, S., Moghaddam, M., Tabatabaeejad, A., Member, S., Jaruwatanadilok, S., et al. (2018). Spatial and temporal variability of root-zone soil moisture acquired from hydrologic modeling and AirMOSS P-Band radar. *IEEE Journal of Selected Topics in Applied Earth Observations and Remote Sensing*, 11(12), 1–13. <https://doi.org/10.1109/JSTARS.2018.2865251>
- de Saint-Venant, B. (1871). Theory of unsteady water flow with application to floods and to propagation of tides in river channels. *Proceedings of French Academy of Science*, 73, 148–154.
- De Schepper, G., Therrien, R., Refsgaard, J. C., & Hansen, A. L. (2015). Simulating coupled surface and subsurface water flow in a tile-drained agricultural catchment. *Journal of Hydrology*, 521, 374–388. <https://doi.org/10.1016/j.jhydrol.2014.12.035>
- Drake, C. W., Jones, C. S., Schilling, K. E., Amado, A. A., & Weber, L. J. (2018). Estimating nitrate-nitrogen retention in a large constructed wetland using high-frequency, continuous monitoring and hydrologic modeling. *Ecological Engineering*, 117, 69–83. <https://doi.org/10.1016/j.ecoleng.2018.03.014>
- Ek, M. B., Mitchell, K. E., Lin, Y., Rogers, E., Grunmann, P., Koren, V., et al. (2003). Implementation of Noah land surface model advances in the National Centers for Environmental Prediction operational mesoscale Eta model. *Journal of Geophysical Research*, 108(D22), 8851. <https://doi.org/10.1029/2002JD003296>
- Foley, J. A., Prentice, I. C., Ramankutty, N., Levis, S., Pollard, D., Sitch, S., & Haxeltine, A. (1996). An integrated biosphere model of land surface processes, terrestrial carbon balance, and vegetation dynamics. *Global Biogeochemical Cycles*, 10(4), 603–628. <https://doi.org/10.1029/96GB02692>
- Francesconi, W., Smith, D. R., Heathman, G. C., Wang, X., & Williams, C. O. (2014). Monitoring and APEX Modeling of no-till and reduced-till in tile-drained agricultural landscapes for water quality. *Transactions of the American Society of Agricultural and Biological Engineers*, 57(3), 777–789. <https://doi.org/10.13031/trans.57.10332>
- Frank, S., Fürst, C., Koschke, L., & Makeschin, F. (2012). A contribution towards a transfer of the ecosystem service concept to landscape planning using landscape metrics. *Ecological Indicators*, 21, 30–38. <https://doi.org/10.1016/j.ecolind.2011.04.027>
- Gassman, P. W., Williams, J. R., Wang, X., Saleh, A., Osei, E., Hauck, L. M., et al. (2010). The Agricultural Policy/Environmental eXtender (APEX) Model: An emerging tool for landscape and watershed environmental analyses. *Transactions of the American Society of Agricultural and Biological Engineers*, 53(3), 711–740. <https://doi.org/10.13031/2013.30078>
- Gil, Y., Garijo, D., Khider, D., Knoblock, C. A., Ratnakar, V., Osorio, M., et al. (2021). Artificial intelligence for modeling complex systems: Taming the complexity of expert models to improve decision making. *ACM Transactions on Interactive Intelligent Systems*, 11(2), 1–49. <https://doi.org/10.1145/3453172>
- Griffin, T. S., He, Z., & Honeycutt, C. W. (2005). Manure composition affects net transformation of nitrogen from dairy manures. *Plant and Soil*, 273(1), 29–38. <https://doi.org/10.1007/s11104-004-6473-5>

- Groffman, P. M., Butterbach-Bahl, K., Fulweiler, R. W., Gold, A. J., Morse, J. L., Stander, E. K., et al. (2009). Challenges to incorporating spatially and temporally explicit phenomena (hotspots and hot moments) in denitrification models. *Biogeochemistry*, 93(1), 49–77. <https://doi.org/10.1007/s10533-008-9277-5>
- Hill, A. R., Devito, K. J., & Vidon, P. G. (2014). Long-term nitrate removal in a stream riparian zone. *Biogeochemistry*, 121(2), 425–439. <https://doi.org/10.1007/s10533-014-0010-2>
- Hindmarsh, A. C., Brown, P. N., Grant, K. E., Lee, S. L., Serban, R., Shumaker, D. E., & Woodward, C. S. (2005). SUNDIALS: Suite of nonlinear and differential/algebraic equation solvers. *ACM Transactions on Mathematical Software*, 31(3), 363–396. <https://doi.org/10.1145/1089014.1089020>
- Hirt, C. C., Veith, T. L., Collick, A. S., Yetter, S. E., & Brooks, R. P. (2020). Headwater stream condition and nutrient runoff: Relating SWAT to empirical ecological measures in an agricultural watershed in Pennsylvania. *Journal of Environmental Quality*, 49(3), 557–568. <https://doi.org/10.1002/jeq2.20032>
- Hladik, M. L., & Kolpin, D. W. (2015). First national-scale reconnaissance of neonicotinoid insecticides in streams across the USA. *Environmental Chemistry*, 13(1), 12–20. <https://doi.org/10.1071/EN15061>
- Jacob, D., Petersen, J., Eggert, B., Alias, A., Christensen, O. B., Bouwer, L. M., et al. (2014). EURO-CORDEX: New high-resolution climate change projections for European impact research. *Regional Environmental Change*, 14(2), 563–578. <https://doi.org/10.1007/s10113-013-0499-2>
- Jepsen, S. M., Harmon, T. C., & Shi, Y. (2016). Watershed model calibration to the base flow recession curve with and without evapotranspiration effects. *Water Resources Research*, 52(4), 2919–2933. <https://doi.org/10.1002/2015WR017827>
- Katul, G., Manzoni, S., Palmroth, S., & Oren, R. (2009). A stomatal optimization theory to describe the effects of atmospheric CO₂ on leaf photosynthesis and transpiration. *Annals of Botany*, 105(3), 431–442. <https://doi.org/10.1093/aob/mcp292>
- Kemarian, A. R., Duckworth, P., & Williams, J. R. (2009). A spatially distributed modeling approach for precision conservation and agroecosystem design. In *Proceedings 2nd Biennial international symposium farming systems design* (pp. 153–154).
- Kemarian, A. R., Shi, Y., White, C. M., Montes, F., Stöckle, C. O., Huggins, D. R., et al. (2022). The cycles agroecosystem model: Fundamentals, testing, and applications. SSRN. <https://doi.org/10.2139/ssrn.4188402>
- Kemarian, A. R., & Stöckle, C. O. (2010). C-farm: A simple model to evaluate the carbon balance of soil profiles. *European Journal of Agronomy*, 32(1), 22–29. <https://doi.org/10.1016/j.eja.2009.08.003>
- Kemarian, A. R., Stöckle, C. O., & Huggins, D. R. (2005). Transpiration-use efficiency of barley. *Agricultural and Forest Meteorology*, 130(1), 1–11. <https://doi.org/10.1016/j.agrformet.2005.01.003>
- Kim, N. W., Chung, I. M., Won, Y. S., & Arnold, J. G. (2008). Development and application of the integrated SWAT-MODFLOW model. *Journal of Hydrology*, 356(1–2), 1–16. <https://doi.org/10.1016/j.jhydrol.2008.02.024>
- Kirchner, J. W. (2006). Getting the right answers for the right reasons: Linking measurements, analyses, and models to advance the science of hydrology. *Water Resources Research*, 42(3), W03S04. <https://doi.org/10.1029/2005WR004362>
- Koch, J., Cornelissen, T., Fang, Z., Bogena, H., Diekkrüger, B., Kollet, S., & Stisen, S. (2016). Inter-comparison of three distributed hydrological models with respect to seasonal variability of soil moisture patterns at a small forested catchment. *Journal of Hydrology*, 533, 234–249. <https://doi.org/10.1016/j.jhydrol.2015.12.002>
- Kucharik, C. J., Foley, J. A., Delire, C., Fisher, V. A., Coe, M. T., Lenters, J. D., et al. (2000). Testing the performance of a dynamic global ecosystem model: Water balance, carbon balance, and vegetation structure. *Global Biogeochemical Cycles*, 14(3), 795–825. <https://doi.org/10.1029/1999GB001138>
- Kuffour, B. N. O., Engdahl, N. B., Woodward, C. S., Condon, L. E., Kollet, S., & Maxwell, R. M. (2020). Simulating coupled surface–subsurface flows with ParFlow v3.5.0: Capabilities, applications, and ongoing development of an open-source, massively parallel, integrated hydrologic model. *Geoscientific Model Development*, 13(3), 1373–1397. <https://doi.org/10.5194/gmd-13-1373-2020>
- Kumar, M., Bhatt, G., & Duffy, C. J. (2010). An object-oriented shared data model for GIS and distributed hydrologic models. *International Journal of Geographical Information Science*, 24(7), 1061–1079. <https://doi.org/10.1080/13658810903289460>
- Leonard, L., & Duffy, C. J. (2014). Automating data-model workflows at a level 12 HUC scale: Watershed modeling in a distributed computing environment. *Environmental Modelling & Software*, 61, 174–190. <https://doi.org/10.1016/j.envsoft.2014.07.015>
- Lu, H., Bryant, R. B., Buda, A. R., Collick, A. S., Folmar, G. J., & Kleinman, P. J. A. (2015). Long-term trends in climate and hydrology in an agricultural, headwater watershed of central Pennsylvania, USA. *Journal of Hydrology: Regional Studies*, 4, 713–731. <https://doi.org/10.1016/j.ejrh.2015.10.004>
- McConnell, C. A., Kaye, J. P., & Kemarian, A. R. (2020). Reviews and syntheses: Ironing out wrinkles in the soil phosphorus cycling paradigm. *Biogeosciences*, 17(21), 5309–5333. <https://doi.org/10.5194/bg-17-5309-2020>
- McLellan, E. L., Cassman, K. G., Eagle, A. J., Woodbury, P. B., Sela, S., Tonitto, C., et al. (2018). The Nitrogen balancing act: Tracking the environmental performance of food production. *BioScience*, 68(3), 194–203. <https://doi.org/10.1093/biosci/bix164>
- Molling, C. C., Strikwerda, J. C., Norman, J. M., Rodgers, C. A., Wayne, R., Morgan, C. L., et al. (2005). Distributed runoff formulation designed for a precision agricultural landscape modeling system. *Journal of the American Water Resources Association*, 41(6), 1289–1313. <https://doi.org/10.1111/j.1752-1688.2005.tb03801.x>
- Pabich, W. J., Valiela, I., & Hemond, H. F. (2001). Relationship between DOC concentration and vadose zone thickness and depth below water table in groundwater of Cape Cod, USA. *Biogeochemistry*, 55(3), 247–268. <https://doi.org/10.1023/A:1011842918260>
- PASDA. (2022). Pennsylvania spatial data access. Retrieved from <https://www.pasda.psu.edu/>
- Pineux, N., Lisein, J., Swerts, G., Biélders, C. L., Lejeune, P., Colinet, G., & Degré, A. (2017). Can DEM time series produced by UAV be used to quantify diffuse erosion in an agricultural watershed? *Geomorphology*, 280, 122–136. <https://doi.org/10.1016/j.geomorph.2016.12.003>
- Pionke, H. B., Gburek, W. J., & Sharpley, A. N. (2000). Critical source area controls on water quality in an agricultural watershed located in the Chesapeake Basin. *Ecological Engineering*, 14(4), 325–335. [https://doi.org/10.1016/S0925-8574\(99\)00059-2](https://doi.org/10.1016/S0925-8574(99)00059-2)
- Pokhrel, P., & Gupta, H. V. (2010). On the use of spatial regularization strategies to improve calibration of distributed watershed models. *Water Resources Research*, 46(1), W01505. <https://doi.org/10.1029/2009WR008066>
- Pravia, M. V., Kemarian, A. R., Terra, J. A., Shi, Y., Macedo, I., & Goslee, S. (2019). Soil carbon saturation, productivity, and carbon and nitrogen cycling in crop-pasture rotations. *Agricultural Systems*, 171(December 2017), 13–22. <https://doi.org/10.1016/j.agsy.2018.11.001>
- Qu, Y., & Duffy, C. J. (2007). A semidiscrete finite volume formulation for multiprocess watershed simulation. *Water Resources Research*, 43(8), W08419. <https://doi.org/10.1029/2006WR005752>
- Redder, B. W., Kennedy, C. D., Buda, A. R., Folmar, G., & Boyer, E. W. (2021). Groundwater contributions of flow and nitrogen in a headwater agricultural watershed. *Hydrological Processes*, 35(5), e14179. <https://doi.org/10.1002/hyp.14179>
- Rodell, M., Houser, P. R., Jambor, U., Gottschalck, J., Mitchell, K., Meng, C.-J., et al. (2004). The global land data assimilation system. *Bulletin of the American Meteorological Society*, 85(3), 381–394. <https://doi.org/10.1175/BAMS-85-3-381>

- Saarikko, R. A. (2000). Applying a site based crop model to estimate regional yields under current and changed climates. *Ecological Modelling*, 131(2), 191–206. [https://doi.org/10.1016/S0304-3800\(00\)00257-X](https://doi.org/10.1016/S0304-3800(00)00257-X)
- Saha, D., Kaye, J. P., Bhowmik, A., Bruns, M. A., Wallace, J. M., & Kemanian, A. R. (2021). Organic fertility inputs synergistically increase denitrification-derived nitrous oxide emissions in agroecosystems. *Ecological Applications*, 31(7), e02403. <https://doi.org/10.1002/eap.2403>
- Saha, D., Rau, B. M., Kaye, J. P., Montes, F., Adler, P. R., & Kemanian, A. R. (2017). Landscape control of nitrous oxide emissions during the transition from conservation reserve program to perennial grasses for bioenergy. *GCB Bioenergy*, 9(4), 783–795. <https://doi.org/10.1111/gcbb.12395>
- Shi, Y., Baldwin, D. C., Davis, K. J., Yu, X., Duffy, C. J., & Lin, H. (2015). Simulating high-resolution soil moisture patterns in the Shale Hills watershed using a land surface hydrologic model. *Hydrological Processes*, 29(21), 4624–4637. <https://doi.org/10.1002/hyp.10593>
- Shi, Y., Davis, K. J., Duffy, C. J., & Yu, X. (2013). Development of a coupled land surface hydrologic model and evaluation at a critical zone observatory. *Journal of Hydrometeorology*, 14(5), 1401–1420. <https://doi.org/10.1175/JHM-D-12-0145.1>
- Shi, Y., Davis, K. J., Zhang, F., & Duffy, C. J. (2014). Evaluation of the parameter sensitivities of a coupled land surface hydrologic model at a critical zone observatory. *Journal of Hydrometeorology*, 15(1), 279–299. <https://doi.org/10.1175/JHM-D-12-0177.1>
- Shi, Y., Eissenstat, D. M., He, Y., & Davis, K. J. (2018). Using a spatially-distributed hydrologic biogeochemistry model with a nitrogen transport module to study the spatial variation of carbon processes in a Critical Zone Observatory. *Ecological Modelling*, 380, 8–21. <https://doi.org/10.1016/j.ecolmodel.2018.04.007>
- Shi, Y., & Kemanian, A. R. (2022). Cycles-L v1.0.0 [software]. Zenodo. <https://doi.org/10.5281/zenodo.7942338>
- Stafford, J. V. (2000). Implementing precision agriculture in the 21st century. *Journal of Agricultural Engineering Research*, 76(3), 267–275. <https://doi.org/10.1006/jaer.2000.0577>
- Stöckle, C. O., & Kemanian, A. R. (2020). Can crop models identify critical gaps in genetics, environment, and management interactions? *Frontiers in Plant Science*, 11, 737. <https://doi.org/10.3389/fpls.2020.00737>
- Stöckle, C. O., Kemanian, A. R., Nelson, R. L., Adam, J. C., Sommer, R., & Carlson, B. (2014). CropSyst model evolution: From field to regional to global scales and from research to decision support systems. *Environmental Modelling & Software*, 62, 361–369. <https://doi.org/10.1016/j.envsoft.2014.09.006>
- Tague, C. L., & Band, L. E. (2004). RHESSys: Regional hydro-ecologic simulation system—An object-oriented approach to spatially distributed modeling of carbon, water, and nutrient cycling. *Earth Interactions*, 8(19), 1–42. [https://doi.org/10.1175/1087-3562\(2004\)8\(1:RRHSSO\)2.0.CO;2](https://doi.org/10.1175/1087-3562(2004)8(1:RRHSSO)2.0.CO;2)
- Tarboton, D. G. (2015). TauDEM-terrain analysis using digital elevation models. Version 5. Retrieved from <https://hydrology.usu.edu/taudem/taudem5/index.html>
- Tarboton, D. G., Bras, R. L., & Rodriguez-Iturbe, I. (1991). On the extraction of channel networks from digital elevation data. *Hydrological Processes*, 5(1), 81–100. <https://doi.org/10.1002/hyp.3360050107>
- Tarboton, D. G., Schreuders, K. A. T., Watson, D. W., & Baker, M. E. (2009). Generalized terrain-based flow analysis of digital elevation models. In *Proceedings of the 18th world IMACS congress and MODSIM09 international congress on modelling and simulation*, Cairns, Australia (Vol. 2000–2006, pp. 2377–2383).
- Tenreiro, T. R., García-Vila, M., Gómez, J. A., Jimenez-Berni, J. A., & Fereres, E. (2020). Water modelling approaches and opportunities to simulate spatial water variations at crop field level. *Agricultural Water Management*, 240, 106254. <https://doi.org/10.1016/j.agwat.2020.106254>
- USDA-NRCS. (2012). Assessment of the effects of conservation practices on cultivated cropland in the Upper Mississippi river basin (revised CEAP report 2012) (technical report).
- Van Liew, M. W., Wortmann, C. S., Moriasi, D. N., King, K. W., Flanagan, D. C., Veith, T. L., et al. (2017). Evaluating the APEX model for simulating streamflow and water quality on ten Agricultural watersheds in the U.S. *Transactions of the American Society of Agricultural and Biological Engineers*, 60(1), 123–146. <https://doi.org/10.13031/trans.11903>
- Veith, T. L., Richards, J. E., Goslee, S. C., Collick, A. S., Bryant, R. B., Miller, D. A., et al. (2015). Navigating spatial and temporal complexity in developing a long-term land use database for an agricultural watershed. *Journal of Soil and Water Conservation*, 70(5), 288–296. <https://doi.org/10.2489/jswc.70.5.288>
- Wallace, C. D., Sawyer, A. H., Soltanian, M. R., & Barnes, R. T. (2020). Nitrate removal within heterogeneous riparian aquifers under tidal influence. *Geophysical Research Letters*, 47(10), e2019GL085699. <https://doi.org/10.1029/2019GL085699>
- Wallner, M., Haberlandt, U., & Dietrich, J. (2012). Evaluation of different calibration strategies for large scale continuous hydrological modelling. *Advances in Geosciences*, 31, 67–74. <https://doi.org/10.5194/adgeo-31-67-2012>
- Wang, C., Hou, J., Miller, D., Brown, I., & Jiang, Y. (2019). Flood risk management in sponge cities: The role of integrated simulation and 3D visualization. *International Journal of Disaster Risk Reduction*, 39, 101139. <https://doi.org/10.1016/j.ijdrr.2019.101139>
- Wang, X., Kemanian, A. R., & Williams, J. R. (2011). Special features of the EPIC and APEX modeling package and procedures for parameterization, calibration, validation, and applications. In L. R. Ahuja & L. Ma (Eds.), *Methods of introducing system models into agricultural research* (pp. 177–208). John Wiley & Sons, Ltd. <https://doi.org/10.2134/advagricsystemodel2.c6>
- Ward, N. K., Maureira, F., Stöckle, C. O., Brooks, E. S., Painter, K. M., Yourek, M. A., & Gasch, C. K. (2018). Simulating field-scale variability and precision management with a 3D hydrologic cropping systems model. *Precision Agriculture*, 19(2), 293–313. <https://doi.org/10.1007/s11119-017-9517-6>
- Wei, X., Bailey, R. T., Records, R. M., Wible, T. C., & Arabi, M. (2019). Comprehensive simulation of nitrate transport in coupled surface-subsurface hydrologic systems using the linked SWAT-MODFLOW-RT3D model. *Environmental Modelling & Software*, 122, 104242. <https://doi.org/10.1016/j.envsoft.2018.06.012>
- Wigmosta, M. S., & Lettenmaier, D. P. (1999). A comparison of simplified methods for routing topographically driven subsurface flow. *Water Resources Research*, 35(1), 255–264. <https://doi.org/10.1029/1998WR900017>
- Williams, J. R. (1990). The erosion-productivity impact calculator (EPIC) model: A case history. *Philosophical Transactions of the Royal Society of London. Series B: Biological Sciences*, 329(1255), 421–428. <https://doi.org/10.1098/rstb.1990.0184>
- Williams, M. R., Buda, A. R., Elliott, H. A., Singha, K., & Hamlett, J. (2015). Influence of riparian seepage zones on nitrate variability in two agricultural headwater streams. *Journal of the American Water Resources Association*, 51(4), 883–897. <https://doi.org/10.1111/1752-1688.12335>
- Woodbury, P. B., Kemanian, A. R., Jacobson, M., & Langholtz, M. (2018). Improving water quality in the Chesapeake Bay using payments for ecosystem services for perennial biomass for bioenergy and biofuel production. *Biomass and Bioenergy*, 114, 132–142. <https://doi.org/10.1016/j.biombioe.2017.01.024>
- Wösten, J. H. M., Lilly, A., Nemes, A., & Le Bas, C. (1999). Development and use of a database of hydraulic properties of European soils. *Geoderma*, 90(3–4), 169–185. [https://doi.org/10.1016/S0016-7061\(98\)00132-3](https://doi.org/10.1016/S0016-7061(98)00132-3)

- Xia, Y., Mitchell, K., Ek, M., Sheffield, J., Cosgrove, B., Wood, E., et al. (2012). Continental-scale water and energy flux analysis and validation for the North American land data assimilation system project phase 2 (NLDAS-2): 1. Intercomparison and application of model products. *Journal of Geophysical Research*, *117*(D3), D03109. <https://doi.org/10.1029/2011JD016048>
- Xiao, D., Shi, Y., Brantley, S. L., Forsythe, B., DiBiase, R., Davis, K., & Li, L. (2019). Streamflow generation from catchments of contrasting lithologies: The role of soil properties, topography, and catchment size. *Water Resources Research*, *55*(11), 9234–9257. <https://doi.org/10.1029/2018WR023736>
- Zhai, Z., Martínez, J. F., Beltran, V., & Martínez, N. L. (2020). Decision support systems for agriculture 4.0: Survey and challenges. *Computers and Electronics in Agriculture*, *170*, 105256. <https://doi.org/10.1016/j.compag.2020.105256>
- Zhang, Y., Li, W., Sun, G., Miao, G., Noormets, A., Emanuel, R., & King, J. S. (2018). Understanding coastal wetland hydrology with a new regional-scale, process-based hydrological model. *Hydrological Processes*, *32*(20), 3158–3173. <https://doi.org/10.1002/hyp.13247>
- Zheng, W., Lamačová, A., Yu, X., Krám, P., Hruška, J., Zahradníček, P., et al. (2021). Assess hydrological responses to a warming climate at the lysina critical zone observatory in central Europe. *Hydrological Processes*, *35*(9), e14281. <https://doi.org/10.1002/hyp.14281>
- Zhi, W., Shi, Y., Wen, H., Saberi, L., Ng, G.-H. C., Sadayappan, K., et al. (2022). BioRT-flux-PIHM v1.0: A biogeochemical reactive transport model at the watershed scale. *Geoscientific Model Development*, *15*(1), 315–333. <https://doi.org/10.5194/gmd-15-315-2022>

Erratum

The originally published version of this article contained typographical errors in Table 3. The third columns, from “1× N” to “1.5× N,” under the heading “Cycled (uncoupled)” should have been placed under the heading “Cycles-L.” The errors have been corrected, and this may be considered the authoritative version of record.